# Novel Bioimaging Techniques using Spectral Information for Monitoring Oxygen Saturation - Evaluated in Human Models of Skin Hypoperfusion

Bunke, Josefine

2024

*Document Version:*
Publisher's PDF, also known as Version of record

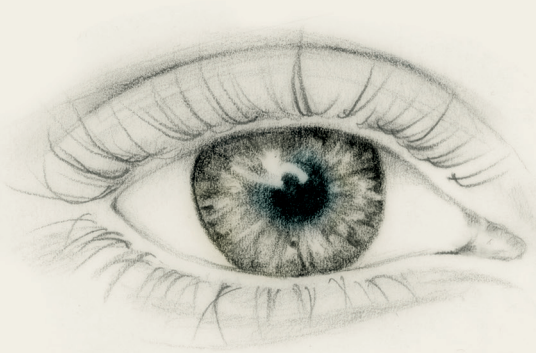

# Novel Bioimaging Techniques using Spectral Information for Monitoring Oxygen Saturation

## Evaluated in Human Models of Skin Hypoperfusion

JOSEFINE BUNKE
DEPARTMENT OF CLINICAL SCIENCES, LUND | FACULTY OF MEDICINE | LUND UNIVERSITY

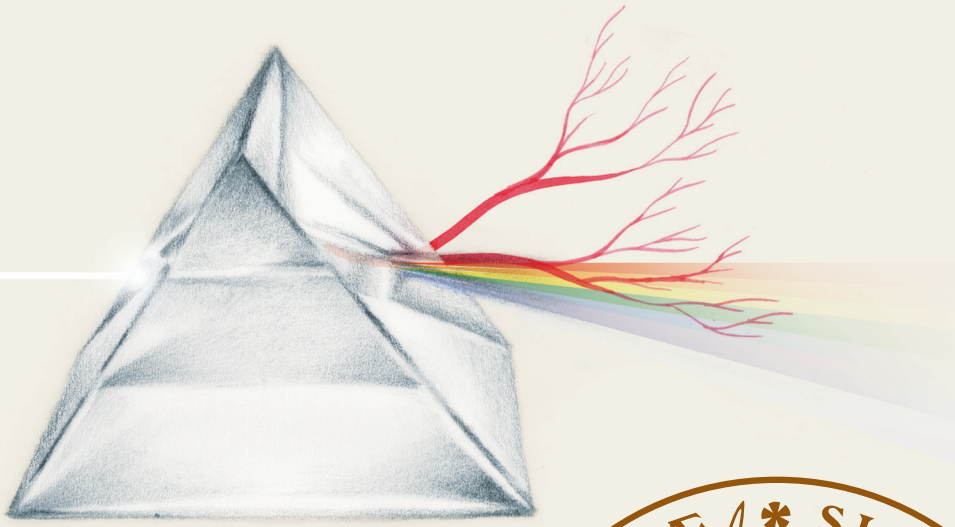

# Novel Bioimaging Techniques using Spectral Information for Monitoring Oxygen Saturation

# Novel Bioimaging Techniques using Spectral Information for Monitoring Oxygen Saturation

## Evaluated in Human Models of Skin Hypoperfusion

Josefine Bunke, MD


LUND
UNIVERSITY

DOCTORAL DISSERTATION

Doctoral dissertation for the degree of Doctor of Philosophy (PhD) at the Faculty of Medicine, Lund University, Sweden. To be defended on October 11th, 2024, at 1 pm in Belfragesalen, Klinikgatan 32, Lund University, Lund, Sweden.

*Faculty opponent*

Professor Richard C. Allen, M.D., Ph.D., Professor, The University of Texas at Austin, Houston, Texas, USA

**Organization:** LUND UNIVERSITY
Faculty of Medicine
Department of Clinical Sciences, Lund
Ophthalmolgy, Lund, Sweden

**Document name:** Doctoral Dissertation
**Date of issue:** 2024-10-11
**Sponsoring organization:**

**Author(s):** Josefine Bunke

**Title and subtitle:** Novel Bioimaging Techniques using Spectral Information for Monitoring Oxygen Saturation - Evaluated in Human Models of Skin Hypoperfusion

**Abstract:**

The measurement of blood perfusion and oxygen saturation ($sO_2$) is crucial to monitor tissue health. Most imaging techniques are currently based on one-point measurements, providing limited information on the surrounding tissue. There is a need of developing new techniques that are easy to use and provide a more comprehensive view of the biological processes. The overall aim of this dissertation was to investigate novel bioimaging techniques including diffuse reflectance spectroscopy (DRS), hyperspectral imaging (HSI), and photoacoustic imaging (PAI) for monitoring the response of hypoperfusion, including $sO_2$, in human skin. Spectral unmixing was evaluated as an analysis method for the spectral information obtained with the bioimaging techniques. An additional aim was to investigate the effect of local anesthesia containing epinephrine by determining the time to maximum effect of epinephrine, and by comparing the effects of a buffered local anesthetic to those of a non-buffered local anesthetic.

Hypoperfusion was obtained by a subcutaneous injection of a local anesthetic containing epinephrine in the forearm or eyelid skin, or by vascular occlusion in a finger. Spectral information obtained from DRS, HSI or PAI was used to monitor $sO_2$ and perfusion. Laser speckle contrast imaging (LSCI) was used as a reference method for monitoring blood perfusion in the eyelid skin.

Extended-wavelength DRS (EW-DRS) could identify the decrease in oxyhemoglobin ($HbO_2$) after injection with lidocaine containing epinephrine. Additionally, EW-DRS identified spectral changes likely due to molecular changes in the tissue.

By creating two dimensional (2D) maps of $sO_2$ and other chromophores, HSI was used to monitor the effect of a local anesthetic containing epinephrine in the human eyelid and forearm skin. LSCI showed a distinct decrease in perfusion in the eyelid skin after the injection of the local anesthetic containing epinephrine, while HSI showed less reduction in $sO_2$.

Depth-resolved mapping with PAI was used to identify the different skin layers in the forearm skin. Additionally, $HbO_2$, deoxyhemoglobin (HbR), melanin and fat could be identified in the various skin layers and the different skin layers were found to react differently concerning $HbO_2$ during vascular occlusion.

The maximum effect of epinephrine in a local anesthetic was found after around 2 min. This is in line with clinical experience and many other studies, although the results differ to some. Additionally, it was found that a buffered local anesthetic caused less pain on injection compared to non-buffered anesthetics, and had a duration of up to 5 h, making it a suitable choice for surgery up to this length.

In conclusion, spectral information and spectral unmixing can be used to identify different chromophores and to monitor $sO_2$ and perfusion in human skin. HSI and PAI have the capacity to produce spatially resolved images in surface and depth, giving a more comprehensive approach for monitoring tissue viability. Full effect of epinephrine in a local anesthetic was found to be approximately 2 min. Further research is needed to explore this topic more extensively and to better understand the effects of epinephrine in local anesthetics.

**Key words:** Bioimaging, oxygenation, oxygen saturation, perfusion, diffuse reflectance spectroscopy, hyperspectral imaging, photoacoustic imaging, spectral unmixing, local anesthesia, epinephrine, buffering.

Classification system and/or index terms (if any)

Supplementary bibliographical information

**ISSN and key title**: 1652-8220

**Language:** English

**ISBN:** 978-91-8021-615-9

**Number of pages**: 78

Recipient's notes

Price

Security classification



Signature

Date 2024-08-15

# Novel Bioimaging Techniques using Spectral Information for Monitoring Oxygen Saturation

## Evaluated in Human Models of Skin Hypoperfusion

Josefine Bunke, MD


LUND
UNIVERSITY

Faculty of Medicine
Department of Clinical Sciences, Lund

ISBN 978-91-8021-615-9
ISSN 1652-8220

Printed in Sweden by Media-Tryck, Lund University
Lund 2024


Media-Tryck is a Nordic Swan Ecolabel certified provider of printed material. Read more about our environmental work at www.mediatryck.lu.se
MADE IN SWEDEN

*To Lovisa, Oscar and Walter*

*Every accomplishment starts with the decision to try*

*-John F. Kennedy*

# Contents

# Abstract

The measurement of blood perfusion and oxygen saturation ($sO_2$) is crucial to monitor tissue health. Most imaging techniques are currently based on one-point measurements, providing limited information on the surrounding tissue. There is a need of developing new techniques that are easy to use and provide a more comprehensive view of the biological processes. The overall aim of this dissertation was to investigate novel bioimaging techniques including diffuse reflectance spectroscopy (DRS), hyperspectral imaging (HSI), and photoacoustic imaging (PAI) for monitoring the response of hypoperfusion, including $sO_2$, in human skin. Spectral unmixing was evaluated as an analysis method for the spectral information obtained with the bioimaging techniques. An additional aim was to investigate the effect of local anesthesia containing epinephrine by determining the time to maximum effect of epinephrine, and by comparing the effects of a buffered local anesthetic to those of a non-buffered local anesthetic.

Hypoperfusion was obtained by a subcutaneous injection of a local anesthetic containing epinephrine in the forearm or eyelid skin, or by vascular occlusion in a finger. Spectral information obtained from DRS, HSI or PAI was used to monitor $sO_2$ and perfusion. Laser speckle contrast imaging (LSCI) was used as a reference method for monitoring blood perfusion in the eyelid skin.

Extended-wavelength diffuse reflectance spectroscopy (EW-DRS) could identify the decrease in oxyhemoglobin ($HbO_2$) after injection with lidocaine containing epinephrine. Additionally, EW-DRS identified spectral changes likely due to molecular changes in the tissue.

By creating two dimensional (2D) maps of $sO_2$ and other chromophores, HSI was used to monitor the effect of a local anesthetic containing epinephrine in the human eyelid and forearm skin. LSCI showed a distinct decrease in perfusion in the eyelid skin after the injection of the local anesthetic containing epinephrine, while HSI showed less reduction in $sO_2$.

Depth-resolved mapping with PAI was used to identify the different skin layers in the forearm skin. Additionally, $HbO_2$, deoxyhemoglobin (HbR), melanin and fat

could be identified in the various skin layers and the different skin layers were found to react differently concerning $HbO_2$ during vascular occlusion.

The maximum effect of epinephrine in a local anesthetic was found after around 2 min. This is in line with clinical experience and many other studies, although the results differ to some. Additionally, it was found that a buffered local anesthetic caused less pain on injection compared to non-buffered anesthetics, and had a duration of up to 5 h, making it a suitable choice for surgery up to this length.

In conclusion, spectral information and spectral unmixing can be used to identify different chromophores and to monitor $sO_2$ and perfusion in human skin. HSI and PAI have the capacity to produce spatially resolved images in surface and depth, giving a more comprehensive approach for monitoring tissue viability. Full effect of epinephrine in a local anesthetic was found to be approximately 2 min. Further research is needed to explore this topic more extensively and to better understand the effects of epinephrine in local anesthetics.

# Papers included in this thesis

I. **Bunke J**, Sheikh R, Reistad N, Malmsjö M. *Extended-wavelength diffuse reflectance spectroscopy for a comprehensive view of blood perfusion and tissue response in human forearm skin.* Microvascular Research. 2019 Jul;124:1-5.

II. **Bunke J**, Merdasa A, Stridh M, Rosenquist P, Berggren J, Hernandez-Palacios JE, Dahlstrand U, Reistad N, Sheikh R, Malmsjö M. *Hyperspectral and laser speckle contrast imaging for monitoring the effect of epinephrine in local anesthetics in oculoplastic surgery.* Ophthalmic Plastic and Reconstructive Surgery. 2022 Sep-Oct 01;38(5):462-468.

III. Gustafsson N, **Bunke J**, Magnusson L, Albinsson J, Hérnandez-Palacios J, Sheikh R, Malmsjö M, Merdasa A. *Optimizing clinical $O_2$ saturation mapping using hyperspectral imaging and diffuse reflectance spectroscopy in the context of epinephrine injection.* Biomedical Optics Express. 2024 Feb 29;15(3):1995-2013.

IV. **Bunke J**, Merdasa A, Sheikh R, Albinsson J, Erlöv T, Gesslein B, Cinthio M, Reistad N, Malmsjö M. *Photoacoustic imaging for the monitoring of local changes in oxygen saturation following an adrenaline injection in human forearm skin.* Biomedical Optics Express. 2021 Jun 15;12(7):4084-4096.

V. Merdasa A, **Bunke J**, Naumovska M, Albinsson J, Erlöv T, Cinthio M, Reistad N, Sheikh R, Malmsjö M. *Photoacoustic imaging of the spatial distribution of oxygen saturation in an ischemia-reperfusion model in humans.* Biomedical Optics Express. 2021 Mar 30;12(4):2484-2495.

VI. **Bunke J**, Sheikh R, Hult J, Malmsjö M. *Buffered local anesthetics reduce injection pain and provide anesthesia for up to 5 hours.* Journal of Plastic, Reconstructive and Aesthetic Surgery. 2018 Aug;71(8):1216-1230.

## Other related paper

Sheikh R, **Bunke J**, Thorisdottir RL, Hult J, Tenland K, Gesslein B, Reistad N, Malmsjö M. *Hypoperfusion following the injection of epinephrine in human forearm skin can be measured by RGB analysis but not with laser speckle contrast imaging.* Microvascular Research. 2019 Jan;121:7-13.

# Abbreviations

| | |
|---|---|
| DRS | Diffuse reflectance spectroscopy |
| EW-DRS | Extended-wavelength diffuse reflectance spectroscopy |
| $HbO_2$ | Oxyhemoglobin |
| HbR | Deoxyhemoglobin |
| HbT | Total hemoglobin |
| HSI | Hyperspectral imaging |
| LDI | Laser Doppler imaging |
| LSCI | Laser speckle contrast imaging |
| NIRS | Near-infrared spectroscopy |
| NRS | Numerical rating scale |
| OCT | Optical coherence tomography |
| PAI | Photoacoustic imaging |
| RGB | Red-green-blue |
| $sO_2$ | Oxygen saturation |
| 2D | Two dimensional |
| 3D | Three dimensional |

# Introduction

The measurement of blood perfusion and oxygen saturation ($sO_2$) is important for monitoring tissue health. In the past, monitoring techniques have been invasive or relied on single-point measurements, offering limited information about the surrounding tissue. There is a need to develop better non-invasive techniques with spatial resolution for monitoring tissue and detecting disease in a comprehensive manner. The studies presented in this dissertation have focused on studying $sO_2$ in models of hypoperfusion in human skin using novel bioimaging techniques. The two models of hypoperfusion include injection with a local anesthetic containing epinephrine and vascular occlusion of a finger.

## Skin anatomy and microcirculation

A better understanding of the anatomy and microcirculation of the skin is needed if we are to understand the effects of hypoperfusion, such as that in response to a local anesthetic containing epinephrine or local vasoconstriction.

*Skin anatomy*

The epidermis is the most superficial layer of the skin, covering nearly the entire body surface, with the primary function of protecting the underlying organs. Its thickness varies greatly depending on anatomical site, for example 50 μm on the eyelids, 75 μm on the volar forearm to almost 1 mm on the soles of the feet [1]. The underlying dermis, which is 2 to 5 mm thick, consists of collagen and elastic fibers embedded in a mucopolysaccharide matrix. Dermal thickness varies depending on the part of the body and the thickest reticular dermis (> 4 mm) is found on the back [2]. Within the dermis, fibroblasts produce connective tissue components, mast cells control immune and inflammatory responses, and melanocytes are responsible for skin pigmentation. The density of melanocytes varies between people, and the different parts of the body. The dermis also contains networks of blood and lymphatic vessels [3]. The hypodermis, also known as the subcutaneous layer, is

located beneath the dermis. It primarily consists of fat and connective tissue, providing insulation and protection of the underlying muscles and organs [4].

Sensory fiber receptors, found in the dermis, transmit information regarding pain (c-fibers), vibration, pressure, and temperature [5]. The many classes of sensory fibers have different diameters and firing rates. For example, pain fibers are more sensitive than those registering pressure and proprioception. These fibers are the reason why a patient can feel a sense of pressure despite complete anesthesia of pain fibers [6]. The lips, tongue, and tips of the fingers are the most sensitive areas of the body [7].

*Microcirculation of the skin*

Small blood vessels that cannot be seen by the naked eye, including small arteries (with diameters < 150 μm), arterioles, capillaries, and venules, are responsible for microcirculation in the skin [8]. Arterioles mainly regulate blood flow and tissue perfusion, while oxygen and nutritional exchange is performed in the capillaries. [9]. Capillaries are extremely narrow, ensuring that erythrocytes flow close to both the vessel wall and the cells of the target organ, facilitating efficient oxygen and nutrient exchange. A typical capillary has a diameter of 4-10 μm. The architecture of the capillary network varies between tissues; for example, in the skin, which has low metabolic activity, the capillary density ranges 16-55/mm². In contrast, muscles, with their high metabolic demands, have a much higher capillary density of 1000-2000/mm² [10].

The microcirculation has several important functions, such as regulating skin homeostasis, controlling the transfer of molecules and cells between the blood and the tissue, regulating blood flow, thermoregulation of the skin, and managing inflammatory responses. Spontaneous contractions and vasodilation of the microvascular bed, known as vasomotion, cause fluctuations in blood flow approximately 4 times per min [11]. The circulation can thus be adjusted and directed to specific organs depending on needs, such as the stomach and intestines after a meal. Vascular resistance, and thus blood flow, are influenced by nerve signals, local chemical mediators such as histamine and nitric oxide, and local oxygen levels [12]. Smooth muscle cells in the arterioles enable changes in perfusion. While normal blood flow is typically around 0.25 L/min, it can reach up to 8 L/min during intense exercise, ensuring oxygen delivery to the muscles and aiding in body temperature regulation [13].

The microcirculation in human skin is organized in two plexuses parallel to the skin surface. The superficial vascular plexus, located in the papillary dermis, consists of small arterioles and venules with perpendicular capillary loops extending toward the

surface, supporting skin nutrition [14]. The deep vascular plexus is found deeper down in the dermal-hypodermal interface and consists of larger-caliber vessels stemming from the underlying muscle and adipose tissue. These vessels form ascending arterioles and descending venules, connecting to the superficial plexus [15]. Ascending arterioles are spaced randomly, but approximately every 1.5 mm, branching to form microvascular networks around sweat glands and hair follicles (Figure 1).

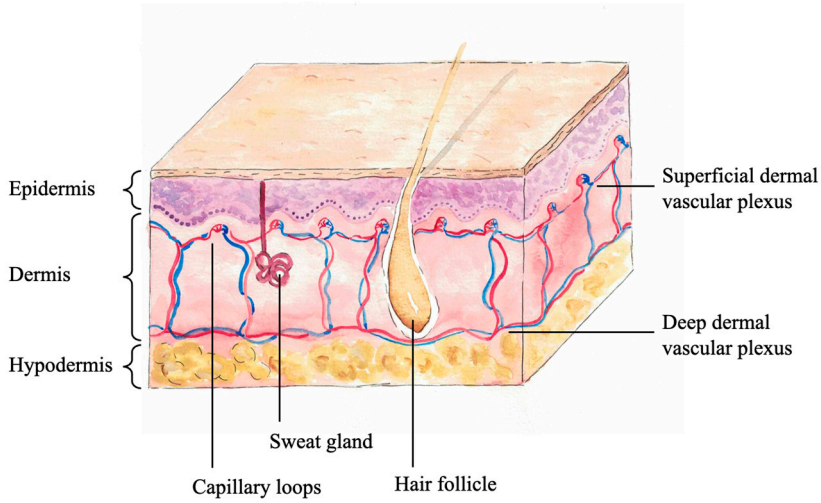


**Figure 1. Skin anatomy.**
The image shows the epidermis, dermis, and hypodermis. The microcirculation is organized with a superficial dermal plexus with perpendicular capillary loops ascending towards the surface and deep dermal vascular plexuses. Sweat glands and hair follicles are found in the dermis. (Illustration by Emilia Johansson)

*Eyelid anatomy and vascularization*

The eyelid is an important and unique structure that protects the eye and helps maintain its moisture. It is composed of two main structural layers known as the outer and inner lamellae. The outer lamella is the anterior portion of the eyelid and consists primarily of skin and muscle while the inner lamella is the posterior portion, made up of the tarsal plate and conjunctiva [16]. The eyelid skin is different from that of the rest of the body in that it lacks a distinct hypodermis [17]. However, the absence of a hypodermis in the eyelid allows for a thinner and more flexible structure able to move smoothly over the surface of the eye.

The eyelid is also a particularly well perfused region with several blood supplies. The internal carotid artery branches into the ophthalmic artery, which supplies blood to the eyelids. The external carotid artery contributes to the blood supply of the

eyelids through its branches: the infraorbital, facial, and superficial arteries. These arteries form branches and anastomoses, creating arcades such as the marginal and peripheral arcades in the upper eyelid, and the lower palpebral arcade in the lower eyelid [16] (Figure 2).

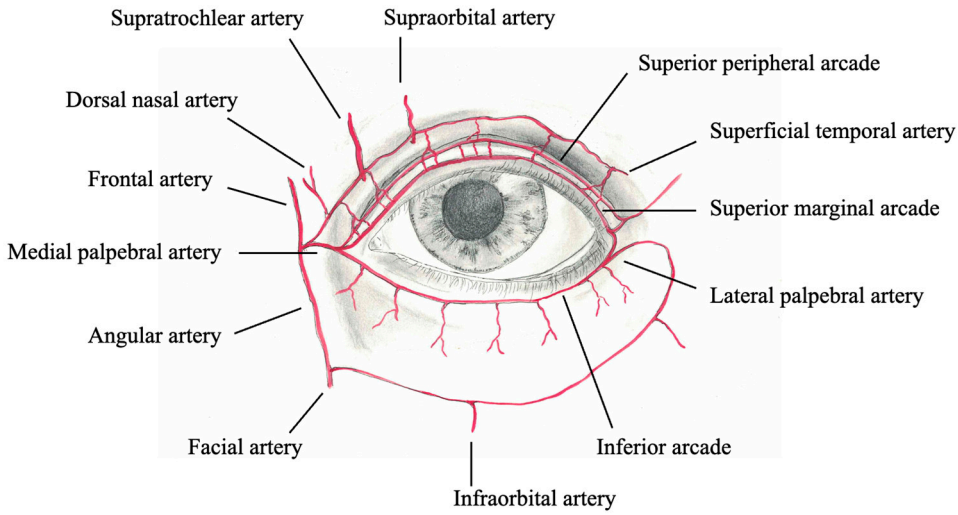


**Figure 2. Eyelid vascularization.**
The image shows the rich vascularization of the eyelid with several arcades. (Illustration by Emilia Johansson)

# The importance of mapping perfusion and oxygenation

Perfusion and $sO_2$ are important variables in assessing tissue viability, organ function, and overall patient well-being. Monitoring $sO_2$ provides important information about oxygen delivery to tissues, ensuring cellular metabolism and function. Measuring $sO_2$ aids in diagnosing and managing a wide range of systemic medical conditions, such as cardiovascular diseases, respiratory disorders, sepsis, and shock. Thus, the evaluation of $sO_2$ and perfusion are also important when assessing local conditions where there is a risk of hypoperfusion and ischemia. Local monitoring can be helpful in many surgical and medical conditions, for example in reconstructive flap surgery, skin burns, diabetic foot ulcers, and systemic inflammatory conditions such as Raynaud's phenomenon.

## Bioimaging techniques for reconstructive surgery

Surgical techniques were established many decades ago, long before modern blood monitoring techniques were introduced. Understanding how blood perfusion and $sO_2$ change during and after reconstructive surgery is crucial for predicting the viability of grafts and flaps, preventing ischemia and thus promoting tissue survival. Hypoxia, resulting from inadequate oxygen supply, can lead to tissue necrosis and graft failure.

Reconstructive procedures that have been in use for over a century have relied on clinical observations, such as assessing the color, turgor, smell, temperature, and capillary refill time, to guide the clinician in the assessment of tissue viability. However, the evaluation of tissue status by observation is highly subjective, and requires long clinical experience [18, 19].

Techniques for perfusion monitoring have recently been developed to provide more objective measures than traditional clinical examination. For example near-infrared spectroscopy (NIRS) has been found to recognize a postoperatively threatened flap before clinical findings can be identified [18]. NIRS has also been shown to be able to distinguish the source of vascular thrombosis [20].

Several studies have been conducted on tissue perfusion in reconstructive oculoplastic surgery. Imaging techniques such as laser speckle contrast imaging (LSCI) and hyperspectral imaging (HSI) have been investigated and found to provide detailed information on perfusion and $sO_2$ in flaps and grafts [21-24]. The results of these previous studies have, for example, shown that a tarsoconjunctival flap is not perfused as expected in Hughes procedure [25], and that free composite grafts could be used instead [21, 26, 27]. Modern bioimaging techniques facilitate the systematic evaluation of surgical procedures' impact on $sO_2$ and perfusion [8], enabling refinement of current methods and the development of new surgical methods.

## Bioimaging techniques for other medical conditions

Imaging techniques can be helpful in monitoring surgical procedures but can also play a crucial role in the assessment and management of medical conditions, for example skin burns [28]. Early clinical evaluation of burn depth and area is important for the planning of treatment. It is difficult, even for experienced clinicians, to assess burn depth during the first few days following injury. Biopsy is considered the gold standard for diagnosis of burn depth, but multiple biopsies are commonly required in larger burns with varying burn depth at different sites [29]. Imaging techniques can assist in the assessment of burn depth and in monitoring the progress of healing.

Various techniques such as laser Doppler imaging (LDI), NIRS, and capillary microscopy have been used to aid in the assessment of skin burns [30]. LDI has been shown to be useful in evaluating healing potential and blood flow in burn wounds, but the technique is not in routine use at most burn centers. In contrast to LDI, LSCI can measure perfusion instantly [31].

LDI and LSCI measure perfusion, but many other factors, such as microvascular structure and $sO_2$, are important to give a comprehensive view of skin burns. Recent attempts using novel non-invasive imaging techniques with spatial resolution have shown interesting results. For example, Wang et al. used optical coherence tomography (OCT) angiography, providing the possibility of three dimensional (3D) visualization of the microvascular structure [32].

Diabetic foot ulcers represent another condition where imaging can play a vital role in the management and decision making. As a common and serious complication of diabetes, these ulcers can lead to infection, gangrene, and even amputation if not properly managed. Diabetic foot ulcers are associated with neuropathy and peripheral arterial disease, thus vascular supply and $sO_2$ of the tissue are important factors to consider. In clinic, diabetic ulcers are assessed by visual inspection, Doppler arterial waveforms, together with measurement of the blood pressure in the feet [33]. Computed tomography angiography can assess vascular supply but implies ionizing radiation and there is thus need of further developing non-invasive monitoring methods that are easy to use [33].

OCT offers high-resolution images of tissue microstructure, enabling a detailed evaluation of both the skin and underlying tissues. The technique can also detect microvascular abnormalities in patients with diabetes [34]. However, the main limitation of OCT is the imaging depth, allowing only superficial measurements.

Using wavelengths in the infrared region, NIRS enables a slightly deeper penetration into tissue. NIRS has been shown to monitor wounds by differentiating healing from non-healing in diabetic ulcers [35, 36].

Imaging techniques have potential benefits in the diagnostics and management of skin burns, diabetic foot ulcers and many other conditions. Different techniques have strengths and limitations, and perhaps using several techniques simultaneously could provide a comprehensive evaluation and improved patient outcomes in the future.

# Bioimaging techniques

## History of techniques for measuring perfusion and oxygenation

Traditionally, surgeons have assessed the viability of tissue using subjective signs, which requires experience and has a risk of interindividual variation [19]. A range of techniques, including the use of pharmacological agents, fluorescent dyes, radioactive isotopes, pH monitoring, hydrogen gas clearance, micro dialysis and temperature monitoring, have been tested to more objectively assess perfusion [37]. Unfortunately, these techniques are invasive, unreliable, or inconvenient, and are therefore not suitable for use in the clinical setting.

*Spectroscopy*

Spectroscopy is the study of how light interacts with matter. Spectroscopic methods have many applications in research, industry, and environmental monitoring, including fields such as chemistry, biology, physics, and materials science, and are common in medicine in both clinical and research applications. These methods use information on the structural and compositional properties of tissue to measure medically relevant factors such as blood perfusion and $sO_2$ [38, 39].

Initially, spectroscopy focused on the study of visible light. However, through the work of James Clerk Maxwell in the late 1800s, spectroscopy was expanded to include the entire electromagnetic spectrum, categorized by frequency or wavelength [40]. The electromagnetic spectrum is divided into bands, each named according to the type of electromagnetic waves they contain. These bands, listed from low to high frequency, include radio waves, microwaves, infrared, visible light, ultraviolet, X-rays, and gamma rays.

## Established bioimaging techniques

*Pulse oximetry*

Pulse oximetry is the most commonly used spectroscopic method for measuring $sO_2$ in the clinical setting. The technique is based on comparing the transmittance of light of two different wavelengths in the near-infrared spectral range (660 and 940 nm). As oxyhemoglobin ($HbO_2$) and deoxyhemoglobin (HbR) absorb light differently, the amount of blood present will determine how much light is transmitted at the two different wavelengths. Light that is not absorbed is scattered back from the tissue and measured, allowing the analysis of tissue oxygenation [41, 42]. Although pulse oximetry is convenient to use in everyday practice, it only provides an average measure of $sO_2$ in a specific volume, and lacks the spatial

resolution required to identify heterogeneous tissue oxygenation. Furthermore, since light-skinned people are generally overrepresented in calibration studies, there is an increased risk of health conditions being unrecognized in people with darker skins [43, 44]. To address the problem associated with the variability of melanin in patients, recently developed spectroscopic techniques can be used, such as diffuse reflectance spectroscopy (DRS) and HSI [45, 46]. Further, as spectroscopy often involves only two single wavelengths, there is need for other multi-wavelength techniques to make use of the full potential of the spectrum that can be obtained.

*Other modern bioimaging techniques*

There are several laser-based techniques available for clinical bioimaging such as laser Doppler velocimetry, LDI and LSCI. However, although LSCI has been used clinically in surgical interventions, a drawback of all laser-based methods is the sensitivity to movement artefacts [47].

Other more modern imaging techniques, such as diffuse optical tomography, and blood-oxygen-level-dependent contrast imaging provide more information on the anatomy of the tissue, but also have limitations concerning spatial resolution, depth of imaging, and contrast [48, 49]. The equipment required is generally large, and located in separate premises and is therefore not available in many clinical situations, for example, during surgery.

The techniques available for non-invasive monitoring of the viability of tissue are currently limited and often restricted to single-point measurements. There is thus considerable potential for improving perfusion and $sO_2$ measurement methods and for developing novel bioimaging techniques for monitoring tissue viability.

## Novel non-invasive bioimaging techniques

In the studies presented in this dissertation, several novel techniques that are safe, reproducible, and non-invasive, have been used to monitor the biological response to hypoperfusion. The aim is to develop techniques that can overcome the drawbacks of single-point measurements and instead enable two dimensional (2D) or 3D imaging of tissue.

*Laser speckle contrast imaging*

LSCI is a well-studied and clinically accepted method for measuring perfusion with spatial resolution. In the present work, LSCI was used as a reference method to compare more novel imaging techniques such as HSI.

LSCI was initially developed to measure retinal blood flow in the 1980s [50], and has since been used to monitor glaucoma, retinopathy, and macular degeneration [47, 51]. In 1993, Yamamoto et al. introduced a visual blood flow meter, employing a dynamic laser speckle effect [52]. LSCI has recently been used to evaluate the status of systemic sclerosis by measuring blood flow in Raynaud's phenomenon [53], for measuring cerebral blood flow during neurosurgery [54, 55], and as a method of monitoring perfusion during oculoplastic reconstructive surgery [22, 56, 57]. LSCI has been used to study skin burns and has shown that increased perfusion is correlated with faster healing in the first week following injury [58]. Diabetic ulcers have been studied with LSCI and significant differences between non-ischemic, ischemic and critical-ischemic diabetic ulcers could be seen. This shows the potential for future prediction of wound healing which could aid in choosing the best treatment for the patient [59]. As LSCI measures motion, the main drawback is its sensitivity to motion artefacts [47].

*Diffuse reflectance spectroscopy*

DRS is a spectroscopic technique in which the tissue is illuminated with light, and the diffuse reflected light is collected after interaction with the tissue. DRS offers more spectral information than earlier techniques as it includes more wavelengths. DRS has previously been used to evaluate tissue vitality by measuring the $HbO_2$ [60], the total hemoglobin (HbT) [61], and tissue hydration [62]. A wavelength range in the visible part of the spectrum, from 500 nm to 650 nm, is commonly used in DRS [63]. An extended range of wavelengths has been used in several studies, providing a more comprehensive picture of the molecular composition of tissue, allowing the identification of tumors and peripheral nerves, for example [64-66]. DRS is a non-invasive technique that can provide comprehensive information on the illuminated tissue. The drawbacks of DRS are its limited measurement depth and the small sampling volume, as DRS only measures at one point.

*Hyperspectral imaging*

HSI is a spectroscopic technique that provides mapping of the surface, overcoming the spatial limitation of DRS. HSI is a non-invasive, non-ionizing, contact-free technique that uses a white incandescent light source (broad spectrum). The tissue is illuminated, after which the reflected light is processed to create a map of reflectance spectra. HSI uses continuous ranges of wavelengths in contrast to multispectral imaging which uses more than three chosen wavelength bands [67]. HSI has not yet been implemented in clinical practice but has shown promising results in providing spatial maps of oxygen saturation. HSI has been used, for example, for monitoring $sO_2$ in skin flaps [68], in the lower limbs of patients with peripheral vascular disease [69], as well as assessing diabetic foot ulcers [70-72], as

well as monitoring the effect of epinephrine in local anesthetics in human skin [73]. HSI has also been applied to skin burns and has been shown to be a useful tool with the ability to distinguish burn depth [74] in the near-infrared wavelength region [75].

HSI is a promising technique, providing a 2D overview of a region over time. The drawbacks are the need of knowing what chromophores are to be analyzed and the limited measuring depth [36, 72]. Although commercial devices are available with preprogrammed analysis, they are not yet evaluated for clinical routine.

*Photoacoustic imaging*

Photoacoustic imaging (PAI) is a novel imaging technique combining the advantages of optical and ultrasound imaging. The laser penetrates deeper into the tissue creating images of the tissue in depth and can also make use of the longer wavelengths when analyzing $sO_2$. Light is absorbed by the illuminated tissue, creating a thermoelastic response that causes acoustic waves that are detected by an ultrasound transducer, creating an photoacoustic image [76]. PAI can be used to provide functional information about chromophores in tissue with high spatial resolution. PAI has so far mostly been used in animal studies and has shown potential in imaging burn depth with a cross-sectional view [77], but also clinical applications have been studied. For example, PAI has been used to image the vasculature in human feet, providing a more detailed image of the smaller vasculature than that obtained with traditional duplex ultrasonography [78]. PAI was recently used to study synovial oxygenation in patients with rheumatoid arthritis and in detecting hypoxia in the thickened synovium, associated with less local vascularization and greater disease activity [79].

PAI has a deeper penetration than for example DRS and HSI and can provide depth resolved images (Figure 3). The technique is easy to use, but for reasons of laser safety there is a need for eye protection during measurements.

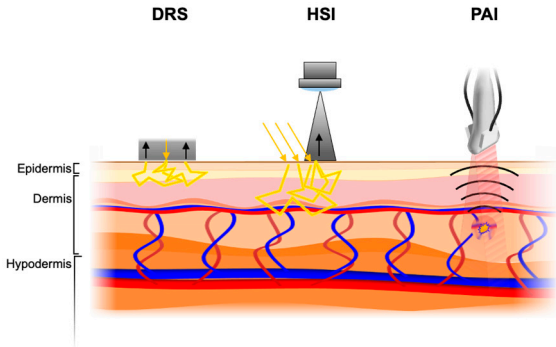


**Figure 3. Schematic overview of novel bioimaging techniques used in this dissertation, regarding imaging modality and depth.**
Images showing a presumable photon path through tissue (yellow). Diffuse reflectance spectroscopy (DRS) is a contact based method with single point illumination. Hyperspectral imaging (HSI) uses more incident photons at different distances from the detector leading to a larger probed volume. DRS and HSI measure at a depth, however they do not provide depth resolution. Photoacoustic imaging (PAI) uses laser light that when absorbed in the tissue will create a thermoelastic response, forming sound waves that can be recorded by the ultrasound probe. The probed depth is deeper with PAI, but more importantly PAI can create a depth resolved image. (Illustration by Aboma Merdasa)

### *Calculation of $sO_2$*

The absorption characteristics of hemoglobin, the primary carrier of oxygen in the blood, are closely related to the oxygenation status of the issue. Hemoglobin has two primary states, $HbO_2$ and HbR, which exhibit distinct optical absorption spectra, particularly in the wavelength region of 550-600 nm, as well as in the near-infrared region where light can penetrate deep into biological tissue [80]. The difference in absorption is used to calculate the distribution of $HbO_2$ and HbR within tissues. The ratio between $HbO_2$ and HbT represents the percentage of hemoglobin that is bound with oxygen in the blood or tissue ($sO_2$), providing a measure of how well oxygen is being transported and used in the tissue.

### *Spectral unmixing*

Spectral unmixing is used to extract the individual spectral signatures, or components, present in a mixed spectrum. When illuminating tissue with light, each type of tissue generates a distinct reflected spectrum based on the specific types and quantities of molecules present. Different chromophores absorb incoming light in varying degrees, while the size and density of the molecules influence light scattering. This combination of absorption and scattering creates a unique spectral signature or “optical fingerprint” for each type of tissue examined. In spectroscopy, the optical fingerprint can be used to reveal which type of tissue or chromophores

are present. Spectral unmixing can be seen as a way of decoding the optical fingerprint. Separating a mixed spectra into the individual components, enables identification of the specific compounds (endmembers) that contribute to the overall signal. In human tissue, some of the spectral signatures are known, for example, those of $HbO_2$, HbR, melanin, fat and water.

# Local anesthesia and epinephrine

The ability of surgeons to perform outpatient surgery is largely dependent on the use of local anesthesia, which has the benefits of simple administration, fast onset, and avoidance of postoperative observation. Adequate anesthesia is of great importance to both surgeons and patients, and factors such as pain on injection, time to onset, and the duration of anesthesia are important to consider [5].

*History of local anesthesia*

In 1884, an Austrian ophthalmologist Carl Koller, at the suggestion of his friend Sigmund Freud, demonstrated cocaine's local anesthetic effect when applied to the eye. This historical event led to the first ocular surgery performed under local anesthesia, and the spread of cocaine as a local anesthetic drug [81].

In the late $19^{th}$ and early $20^{th}$ centuries, safer and more effective synthetic anesthetics were developed. In 1943, a Swedish chemist, Nils Löfgren, synthesized lidocaine [81], which was introduced onto the market in 1948 by the company Astra AB, under the brand name Xylocaine [82].

*Mechanism and properties of local anesthetics*

Local anesthetics reversibly block the action potentials in nerve conduction [83]. The main mechanism of lidocaine is the blockage of the voltage-gated Na+ channels in the cell membranes of sensory and vasomotor nerves [84]. Local anesthetics alone can also have peripheral vascular effects; at low concentrations they induce vasoconstriction, while at higher concentrations they cause vasodilation. However, the vasodilatory effects differs between anesthetics depending on factors such as vascular blood flow, concentration and time after injection [83].

*Epinephrine in local anesthetics*

Epinephrine is often added to local anesthetics to induce vasoconstriction, which reduces bleeding and systemic side effects, as well as prolonging the effect of anesthesia [85]. Local anesthesia with epinephrine is generally considered safe, and has few clinically relevant hemodynamic consequences in patients, even in those

with cardiovascular disease [86-88]. The benefits of adding a vasoconstrictor have also been considered to outweigh potential disadvantages or risks in patients, for example, better effect of the anesthetic and lower endogenous sympathetic tone [88, 89].

During surgery it is important to wait before commencing surgery until vasoconstriction has occurred to reduce perioperative bleeding. The time to onset of anesthesia using lidocaine alone has been well studied [90], and is known to be ≈2 min. The duration of anesthesia is known to be 1 h to 2 h, and the maximum dose of lidocaine alone is 5 mg/kg. Adding epinephrine leads to a faster onset of anesthesia (<2 min), a longer duration, of 2 h to 6 h, and the maximum dose of 7 mg/kg [91].

Although epinephrine is widely used in local anesthetics, there is no clear consensus on the time at which the vasoconstrictive effect has full effect after injection. Surgeons usually wait several minutes for epinephrine to act before commencing surgery, and the optimal delay often stated in textbooks is 7 to 10 min [92]. In a recent review, Bajwa et al. summarized the results of research on the time to vasoconstriction after the administration of local anesthetics with epinephrine [90]. Studies concerning surgical observation of blood loss described stable hypoperfusion after 7 min in the eyelid, and after around 30 min in the upper limb [93, 94]. Results from the non-invasive imaging studies examining perfusion after the injection of a local anesthetic containing epinephrine showed a pooled mean of 5.6 minutes. However, there was great variability across studies, with times ranging from 0.5 to 30 min, perhaps due to differences in imaging techniques and injection sites [90]. Novel bioimaging techniques described in this dissertation have been used to further study the latency of epinephrine in local anesthetics, to address this knowledge gap.

*Buffering local anesthetics*

Solutions of local anesthetics are made acidic to improve their solubility and extend their shelf life. The pH of these solutions is usually between 5.0 and 7.0, which allows them to last 3-4 years. Adjusting the pH closer to the dissociation value (pKa) of the local anesthetic (7.9 for lidocaine) can lead to instability in the uncharged base form. This can cause chemical reactions such as aldehyde formation and photodegradation [95]. Adjusting the pH of local anesthetics, for example by buffering, not only changes the properties of the solution, but can also affect the pain perceived by the patient on injection and infiltration [95].

When epinephrine is added as an adjuvant to local anesthetics, the mixture becomes even more acidic compared to the subcutaneous tissue. Lidocaine with epinephrine

(pH≈6) is 1000 times more acidic than lidocaine alone [96]. Infiltration causes pain, some which may be attributed to the acidity of the anesthetic solution [95]. Buffering the solution is known to reduce the pain on infiltration [96].

Sodium bicarbonate is frequently used to buffer local anesthetics. The addition of bicarbonate increases the pH of the acidic solution closer to the pKa. However, local anesthetics containing high concentrations, of for example lidocaine and epinephrine (>10 mg/ml lidocaine + >10 μg/ml epinephrine), cannot be buffered due to a risk of precipitation [96]. It is therefore not possible to buffer the common combination of high-concentration lidocaine and epinephrine, which is known to provide maximum anesthetic and vasoconstrictive effects [97]. It is a common belief among surgeons that preparations with low concentrations of lidocaine and epinephrine (10 mg/ml lidocaine + 5 μg/ml epinephrine) do not have the same anesthetic effect and duration as preparations with higher concentrations (e.g. 20 mg/ml lidocaine + 12.5 μg/ml epinephrine). The type of surgery, the duration of the procedure, and the risk of bleeding affect the choice of local anesthetic, and surgeons therefore feel that they must choose between more highly concentrated local anesthetics and a weaker buffered one. This has led to a tendency for buffered local anesthetics to be used for short, simple operations, and non-buffered preparations for longer, more complicated operations. However, no systematic studies have been carried out to investigate the properties of weaker buffered local anesthetics vs. stronger non-buffered local anesthetics.

# Aims

The overall aim of this work was to investigate three novel bioimaging techniques including DRS, HSI, and PAI for monitoring hypoperfusion, in human skin. The specific aims were as follows.

To investigate the techniques regarding:

- how spectral information can be used to monitor $sO_2$ and perfusion,
- how the techniques can be used to map $sO_2$ with spatial resolution over the surface and at depth, and
- the evaluation of spectral unmixing for the analysis of $sO_2$.

To investigate the effect of local anesthesia with epinephrine:

- by determining the time to maximum effect of epinephrine, and
- by comparing the effects of a buffered local anesthetic to those of a non-buffered local anesthetic.

# Thesis at a glance

**Table 1. An overview of the aims and methodologies of the studies included in the thesis.**

| Study | Specific study aims | Method | Site | Subjects (n) |
|---|---|---|---|---|
| I | To measure perfusion in tissue upon injection of a local anestetic with epinephrine | EW-DRS | Forearm | Volunteers (9) |
| II | To assess hypoperfusion and $sO_2$ in response to a local anestetic with epinephrine | HSI + LSCI | Eyelid | Patients (9) |
| III | To evaluate DRS and HSI for studying changes in $sO_2$ after injection with a local anesthetic with epinephrine | HSI + DRS | Forearm | Volunteers (12) |
| IV | To monitor $sO_2$ in the skin after injection of a local anesthetic with epinephrine | PAI + DRS | Forearm | Volunteers (7) |
| V | To monitor $sO_2$ during finger ischemia post vascular occlusion | PAI + DRS | Finger | Volunteers (8) |
| VI | To compare pain on injection and the onset and duration of buffered and non-buffered local anesthetics | Pain assessment, tweezer pinch | Forearm | Volunteers (12) |

# Methods

In Studies I-V different combinations of non-invasive bioimaging techniques were used to investigate tissue response to the injection of lidocaine (20 mg/ml) + epinephrine (12.5 μg/ml) in human skin, or during finger occlusion. Different analysis methods were used to monitor and calculate the response to epinephrine and occlusion in terms of perfusion and $sO_2$, and other contributing factors such as melanin, water and fat.

## Laser speckle contrast imaging

*The principle of laser speckle contrast imaging*

LSCI uses near infrared (785 nm) laser beam to create a speckle pattern to measure perfusion in tissue. When the incoming coherent light scatters from the irregular tissue surface, discrepancies arise between the surface and the image plane. The differences in reflection of light will interfere, either constructively or destructively, as seen in Figure 4. The interference of reflected light will then create varying speckle pattern, highly sensitive to motion within the tissue, such as blood flow.

*Laser speckle contrast imaging equipment*

In Study II, blood perfusion was monitored after an injection of a lidocaine (20 mg/ml) + epinephrine (12.5 μg/ml) in the eyelid skin (n=9), using a moorFLP-2 blood flow imager (Moor Instruments Ltd, Devon, UK). The recording rate is up to 100 fps at full field, and the highest achievable spatial resolution at maximum zoom is 3.9 μm per pixel. The perfusion is integrated over 1 sec to optimize the signal-to-noise ratio.

The LSCI speckle patterns were automatically analyzed, and the software of the system calculated the blood perfusion. The results were presented in arbitrary perfusion units. Blood perfusion was calculated as the percentage of the perfusion in the eyelid immediately before injection of the anesthetic. Data from each patient were extracted as a spatial average over a region covering the injected tissue with

sufficient margin in each time frame. The perfusion curve was then normalized to the initial value to allow comparisons to other measurements.

The LSCI equipment used in Study II is CE marked and uses a class 1 laser, which means that it has a low energy output and penetrates only the superficial tissue. It has been approved for use around the eye and does not require eye protection [98].

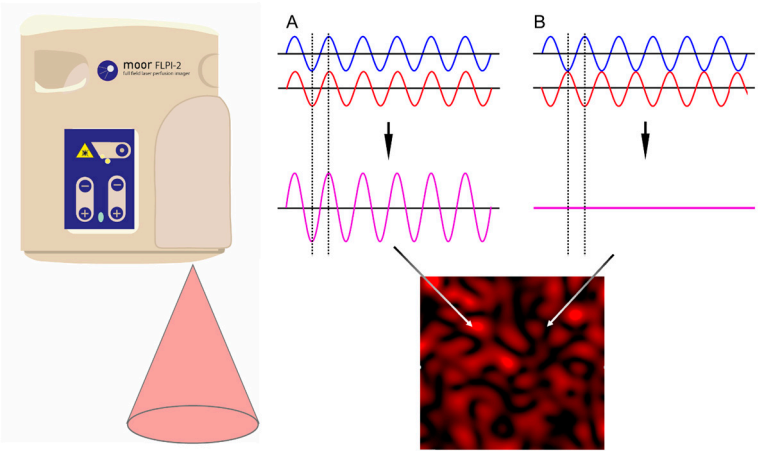


**Figure 4. LSCI equipment and method.**
The laser speckle device with the illuminating infrared laser (785 nm) and an example of how the backscattered light interferes either constructively (A) or destructively (B). This analysis is done pixel by pixel and ultimately generates a speckle pattern below, reflecting the perfusion. (Left illustration by Josefine Bunke)

# Diffuse reflectance spectroscopy

*The principle of diffuse reflectance spectroscopy*

DRS is an optical technique used to analyze the properties of biological tissues by measuring the diffuse reflectance of light for a large range of wavelengths. Light entering biological tissue is reflected, scattered and absorbed in a complicated way as it propagates into the tissue. Biological tissues have a heterogeneous composition, reflected by variations in their optical properties, and reflected light can therefore be analyzed to provide information on the composition of the tissue [99].

A probe consisting of a central light source and a surrounding ring of detection fibers is used to illuminate and detect light. The depth of the measurements depends on several factors, including the wavelength of the light and the source-detector separation. As a result, DRS can be designed to make measurements at specific,

approximate depths [100]. Three different DRS devices were used is this work, and are described below.

*Extended-wavelength diffuse reflectance spectroscopy*

In Study I, a custom-built extended-wavelength diffuse reflectance spectroscopy (EW-DRS) device was used. This technique is based on the overlapping wavelength range of two spectrometers to normalize and combine the two spectra to form one continuous spectrum from 450 to 1550 nm. A portable spectroscopic system that includes a tungsten halogen light source, a contact fiber optic probe (HL-2000-HP; Ocean Optics, Dunedin, FL, USA), and two miniature spectrometers was used to obtain diffuse reflectance spectral signatures. The two spectrometers used in the study resolved light in the visible wavelength range of 350 nm to 1100 nm (QE65000-VIS-NIR; Ocean Optics) and in the near-infrared region of 900 nm to 1700 nm (NIRQuest512; Ocean Optics). The probe used in Study I had a trifurcated fiber bundle with a diameter of 10 mm and a source-detector separation of 2.5 mm (Figure 5).

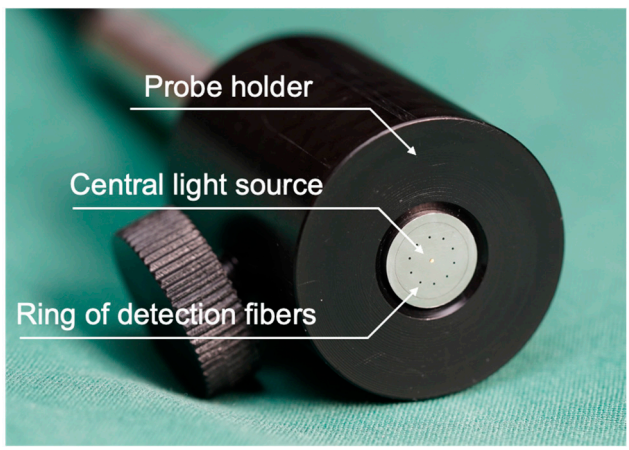


**Figure 5. EW-DRS probe.**
Photograph of the EW-DRS probe showing the probe holder, the central light source and the ring of detection fibers. The distance between the light source and detection fibers is one of the factors affecting the measurement depth of the device.

*Dawson's erythema index*

Dawson's erythema index was used in Study I to monitor the effect of a subcutaneous injection of lidocaine (20 mg/ml) + epinephrine (12.5 µg/ml) in the forearm skin (n=9). Dawson's erythema index was used as a clinical measure to assess the erythema in the skin by accounting the optical properties and also

correcting for melanin. For each spectral measurement E was calculated using the formula as follows Eq (1):

$$E = 100[r + 1.5(q + s) - 2.0(p + t)] \quad (1)$$

where *p, q, r, s* and *t* are logarithm values to base 10 of the logarithm values of the inverse of reflectance of chosen wavelengths (510, 543, 560, 576 and 610 nm) [101].

*The commercial diffuse reflectance spectroscope*

In Studies IV and V, a commercial DRS system (moorVMS-OXY) was used in combination with PAI to monitor the tissue response of lidocaine (20 mg/ml) + epinephrine (12.5 μg/ml) in forearm skin (n=7) and of finger occlusion (n=8).

Photons in the spectral range of 500-650 nm were directed into the tissue via an optical fiber in an excitation probe placed on the skin surface. The light scattered from the skin was collected by another optical fiber placed 1 mm laterally from the excitation probe and detected with a photodiode. The wavelength and separation between the light source and the detector govern the depth of the measurements; greater separation resulting in a greater depth [24]. The DRS system measures a signal integrated over a depth of ≈1 mm into the tissue and operates at a frequency of 1 kHz. Since the signal is an average over the entire volume that is investigated, no vertical spatial information can be obtained from the measurements. The commercial DRS instrument automatically calculates $sO_2$ in percent, and gives $HbO_2$, HbR, and HbT in arbitrary units.

*Vascular occlusion*

In Study V, vascular occlusion was used to induce hypoxia in the fingers of healthy volunteers. A finger cuff was applied and inflated to a pressure exceeding 200 mmHg using a sphygmomanometer (DS-6501-300, Welch Allyn, IL, US) (Figure 6). Measurements were taken with moorVMS-OXY and PAI before, during, and after occlusion, which lasted for 11 min.

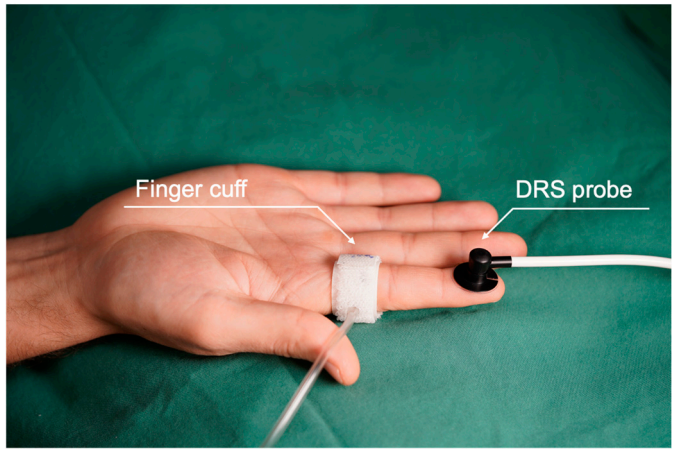


**Figure 6. Commercial DRS (moorVMS-OXY).**
Image of the DRS probe on a fingertip and, in this case, with a finger cuff used for vascular occlusion of the finger in Study V.

*Custom-built diffuse reflectance spectroscope*

A custom-built diffuse reflectance spectroscope, based on the Ocean Insight (QE Pro) spectrometer was used to record absorption spectra from the injection site in Study III. A halogen lamp (HL-2000-FHSA, Ocean Insight Inc.) was connected to the output fibers of a reflectance probe (custom-made, Fiberguide Industries Inc., Caldwell, USA) and the return signal was fed into the spectrometer, which acquired spectra at 20 Hz. Light was directed into the tissue via the output fibers around the circumference of the probe, which was placed in contact with the skin surface. The light scattered from the skin was collected by the fiber in the center of the probe and detected by the spectrometer in the spectral range between 400 and 1000 nm. The probe used has a radius of 5 mm and a source-detector separation of 5 mm, resulting in a detection volume on the order of a few mm into the tissue, which primarily probes the superficial dermis.

# Hyperspectral imaging

*The principle of hyperspectral imaging*

HSI is a technique that combines spectroscopy and imaging, providing a spatially resolved map of the tissue. By acquiring 2D images over a large range of wavelengths (600 nm to 1000 nm), HSI has considerable potential to analyze the structure and composition of biological tissue [99]. HSI collects spectral

information at each pixel in a 2D image creating a 3D dataset of spatial and spectral information, also called a hyperspectral data cube. Outgoing light from the illuminated tissue provides a spectral fingerprint of the specific chromophores present in the tissue [99].

As hyperspectral images are captured at many wavelengths, they provide more detailed spectral information than, for example, standard red-green-blue (RGB) cameras which collect only three wavelengths (Figure 7). RGB cameras capture images with spectral information that corresponds to the sensitivity of human vision. Although this spectral information is not as comprehensive as that obtained with hyperspectral imaging methods, RGB cameras can still be used to qualitatively assess changes in tissue perfusion [102]

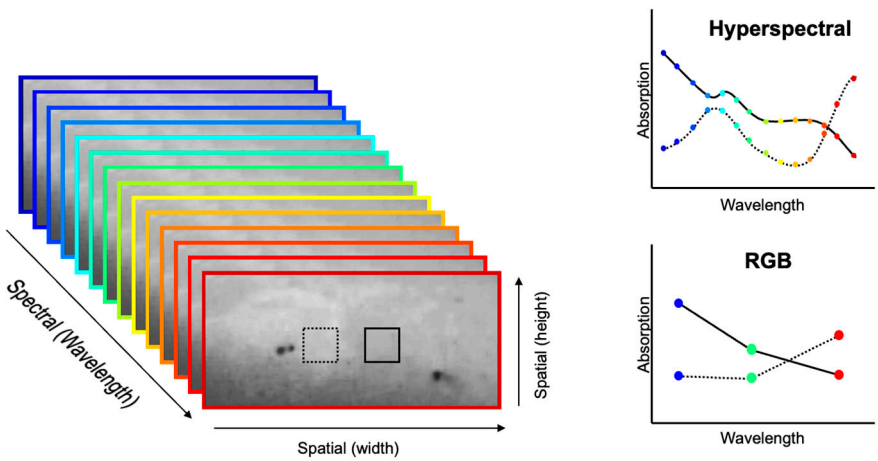


**Figure 7. The principle of HSI compared to an RGB camera.**
Left: Illustration of the way in which HSI captures images at many wavelengths to obtain a spectrum for each pixel in the image. Each image represents a specific narrow range of wavelengths in the electromagnetic spectrum, which is also referred to as a spectral band. These images are then merged to form a 3D hyperspectral data cube where width and hight are the spatial dimensions, and the third dimension is the spectral information. Right: A hyperspectral camera captures images across numerous wavelengths, unlike a RGB camera, which captures images at only three wavelengths. As a result, an hyperspectral camera can produce much more detailed spectral information compared to an RGB camera. (Illustration by Aboma Merdasa)

*Hyperspectral equipment*

In Studies II and III, HSI was used to monitor $sO_2$ in response to injection of lidocaine (20 mg/ml) + epinephrine (12.5 µg/ml) in the forearm skin (n=9 and n=12) using a customized hyperspectral camera in the HySpex model series (Norsk Elektro Optikk AS, Oslo, Norway). The camera acquires hyperspectral images using dispersive methods, which differ from commonly used spectral filtering methods.

This camera can provide high-resolution maps of $sO_2$, by capturing consecutive full 2D images, where each image is filtered to extract a single wavelength (a narrow line in the 2D image), and each point along that line contains the full spectrum. This procedure is repeated by scanning the entire tissue, line-by-line, until the whole area under investigation has been covered.

A halogen lamp was used to illuminate the sample with broad-spectrum white incoherent light (600-1000 nm). The region of interest was scanned, and spectra were collected from each point along a single line that was approximately 10 cm long. Each line generated 640 individual spectra, and the spatial resolution was 150 µm.

A "white reference" was used in the hyperspectral measurements. To normalize the spatial variation of light intensity, a sterile white strip (Tube Holder, 708131, Mölnlycke, Gothenburg, Sweden) was placed in the scanned area, and a separate reference measurement was made against a standard calibrated Spectralon diffuse white reference (WS1, Ocean Insight Inc.). In Figure 8 below, the hyperspectral camera and experimental setup is shown. Linear spectral unmixing (as described below) was applied to each pixel in the measured spectra to determine $sO_2$. In Study III, the effects of injection with lidocaine with epinephrine was compared to those of an injection with saline.

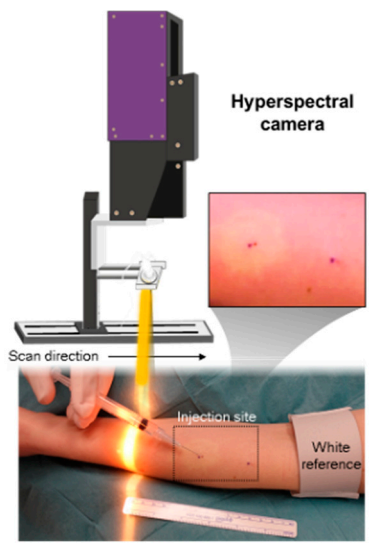


**Figure 8. The hyperspectral camera and experimental setup.**
Schematic showing the hyperspectral camera (top left) where the light source illuminates the arm in the shape of a line across the arm, as shown in the picture below. The hyperspectral camera then scans across the arm, covering both injection sites, as well as the white reference. The inset shows an enhanced image of the injection site demonstrating distinct bleaching of the skin.

# Photoacoustic imaging

*The principle of photoacoustic imaging*

PAI is a technique that combines laser light and ultrasound, with the ability to create spatially resolved images at different depths. PAI is based on the fact that sound scatters less than light. By utilizing the low acoustic scattering in the tissue, deeper propagation of the acoustic signal can be achieved providing an image at greater depths [103]. In PAI, pulses of laser light are emitted into the tissue. The illuminating light with wavelengths in the visible and near infrared region, is absorbed by the tissue, creating a small increase in temperature. This heat creates a thermoelastic response generating acoustic waves that can be detected by the ultrasound transducer (Figure 9). This information can then obtain 3D images with high resolution of the tissue [104].

Chromophores in tissue, such as $HbO_2$, HbR, melanin, fat and water exhibit specific absorption spectra. PAI allows relative quantification of these chromophores at multiple wavelengths [103].

*Photoacoustic equipment*

PAI was performed in Studies IV and V using a Vevo LAZR-X instrument (Visual Sonics Inc., Toronto, ON, Canada), which generates a 7 ns pulse of laser light every 50 ms that is guided onto the skin surface via optical fibers. As these photons penetrate the skin and become absorbed at various depths, depending on the optical properties of the tissue, a thermoelastic response is generated. The acoustic signal is measured with an ultrasound transducer operating at a central frequency of 30 MHz with a bandwidth of 20 - 46 MHz, which provides the spatial contrast. The spectral contrast is obtained by repeating measurements at different excitation wavelengths between 680 nm and 970 nm, in steps of 10 nm, indirectly relating the signal to the light absorption, with 30 spectral components at every point on a vertical cross section. The axial and lateral spatial resolutions are 50 μm and 110 μm, respectively.

The absorption of hemoglobin is associated with the oxygenation status of the tissue. $HbO_2$ and HbR exhibit specific absorption spectra, particularly in the near infrared region. The absorption spectra obtained with PAI can be analyzed by applying spectral unmixing (described below), allowing the extraction of molecular information, including relative concentrations of $HbO_2$ and HbR. In Study III, the value of $sO_2$ calculated for each pixel was mapped onto the original ultrasound image with the same spatial coordinates as the photoacoustic image, to yield a spatially resolved image of the $sO_2$ distribution.

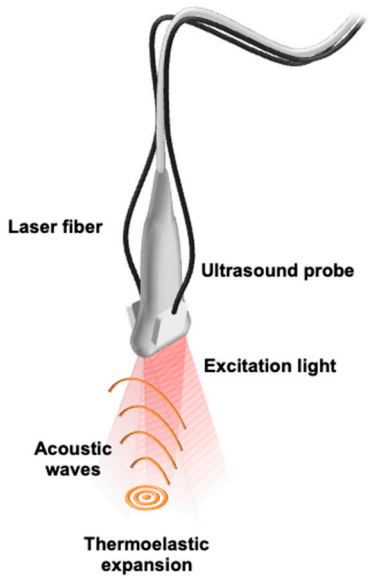


**Figure 9. Schematic setup of the photoacoustic device.**
The photoacoustic probe comprises an ultrasound probe with laser fiberoptic bundles on both sides. When the tissue is irradiated with pulsed laser light, part of the light is absorbed and causes the tissue to undergoe thermoelastic expansion, which in turn generates acoustic waves detected by the ultrasound probe. Hence, light absorption can be measured. (Illustration Aboma Merdasa)

*Safety aspects*

In PAI, the laser is of class 4 which can be potentially harmful and must therefore be used with caution. When using PAI, safety regulations were followed, as previously described by our research group [105]. Moreover, all doors and windows were closed and covered, and the subjects wore protective eye shields throughout the examination. All staff in the examination room wore block-out glasses.

# Spectral unmixing

Spectral unmixing is a method used in spectroscopy to analyze the measured spectral signatures of a tissue into its separate spectral components, known as endmembers, and their corresponding abundances. A spectrum (obtained from for example DRS, HSI or PAI) is a mixture of multiple components. The fundamental assumption behind spectral unmixing is that the total spectrum is a linear or

nonlinear combination of the spectra of the endmembers. The goal is therefore to find out how much of each component the total spectrum is composed of.

In DRS, the total spectra were obtained directly in the measurement. The data preparation process for analysis of HSI or PAI involves either spatially averaging the intensity over a region of the image, or simply extracting the intensity for a single pixel, for each spectral component separately. This procedure is repeated for the same region in each excitation-wavelength-specific image to construct a single spectrum.

A linear spectral unmixing model as described in detail in Study V was used for spectral analysis, according to Eq. (2):

$$M = \sum_{i=1}^{N} a_i s_i + w \quad (2)$$

where $M$ is a vector representing the measured spectrum, $a$ is the linear coefficient (also called the fractional abundance) for each endmember spectrum, and $s$ is a matrix containing the endmember spectra representing the absorption spectra of the tissue constituents assumed to contribute to the measured photoacoustic spectrum, $M$. The only constraint on the linear model is that the coefficients must be positive, which indicates that negative absorption is not a realistic outcome. MATLAB (The MathWorks Inc.) was used to perform a non-negative least-squares approach to minimize the fitting discrepancy by varying the fractional abundance, $a_i$, of each endmember spectrum in $s$. $w$ is a vector accounting for spectral noise.

In determining the endmember spectra, the primary absorptive components in human tissue were assumed to be $HbO_2$ and HbR, melanin, fat, and water (Figure 10). The absorption spectra for each of these endmembers were obtained from a previous report by Jacques et al. [42]. For each specific spectrum, the fractional abundance ($a$) of $HbO_2$ and HbR was used to calculate $sO_2$ according to Eq. (3).

$$sO_2 = \frac{\mathrm{aHb}O_2}{(aHbO_2 + aHbR)} \quad (3)$$

Spectral unmixing of the photoacoustic image is applied to a single spectrum extracted either on a pixel-by-pixel basis, or after averaging many photoacoustic spectra over a specific spatial region.

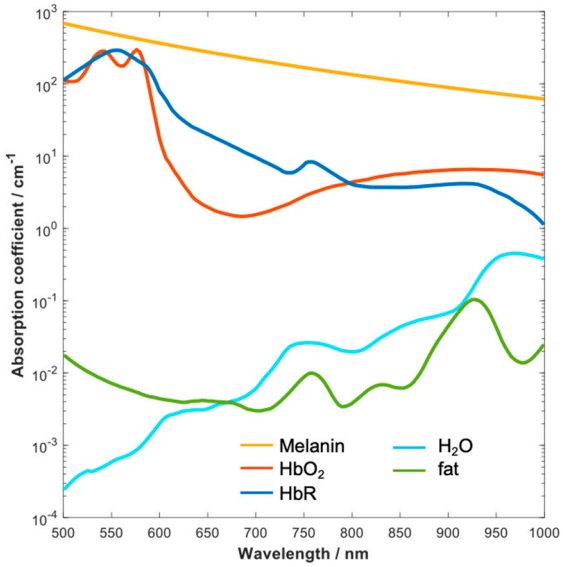


**Figure 10. Specific endmember spectra used in spectral unmixing.**
Different choromphores absorb light in different amounts and at different wavelengths creating a specific absorption spectra. Chromophores including oxyhemoglobin ($HbO_2$), deoxy-hemoglobin (HbR), melanin, fat and water ($H_2O$) are presented with their typical spectra. Spectral unmixing is used to extract these known spectra (endmembers) from a mixed spectrum obtained from the monitored tissue.

# Pain assessment, and onset and duration of local anesthetics

The aim of Study VI was to investigate pain on injection, and the onset and duration of anesthesia using three variations of buffered and non-buffered local anesthetics. The preparations included were buffered lidocaine (10 mg/ml) + epinephrine (5 µg/ml), non-buffered lidocaine (20 mg/ml) + epinephrine (12.5 µg/ml), and non-buffered lidocaine (20 mg/ml). Sodium bicarbonate solution was used as buffer at a ratio of 1:5 (buffer: local anesthetic). A volume of 0.5 ml of each local anesthetic preparation was injected subcutaneously into the forearm of healthy volunteers (Figure 11). The subjects were prepared for the injection but were not allowed to observe the procedure to avoid potentially heightening their perception of pain. Injection pain was estimated by the subjects using a numerical rating scale (NRS) (ranging from 0 to 10 where 0 = no pain and 10 = unbearable pain). The injected sites were then pinched every 30 seconds at each site until the level of pain was rated as zero on three consecutive occasions, to determine the onset of anesthesia.

Pinching was then performed 10 and 20 min after injection, and then every 30 min until sensation had returned, i.e. the pain was scored as greater than 0 using the NRS.

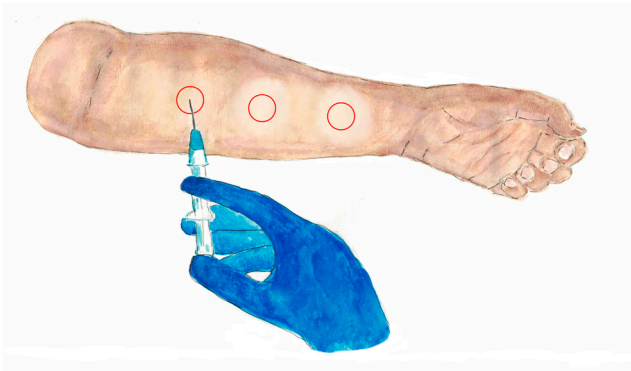

**Figure 11. Experimental setup for assessment of pain, and onset and duration of anesthesia using different local anesthetics solutions.**
Three injections of: buffered lidocaine + epinephrine, non-buffered lidocaine and epinephrine with a higher concentration, and lidocaine alone, were administered subcutaneously in the forearm skin in a randomized order. Pain on injection, and the onset and duration of anesthesia were estimated using a numerical rating scale. (Illustration by Emilia Johansson)

# Data analysis and statistics

In Study I, the forearm skin was monitored with EW-DRS. Statistical analysis was conducted using the Kruskal-Wallis test with Dunn's post hoc test comparing Dawson's erythema index (described above) after injection of a local anesthetic containing epinephrine and saline. Significance was defined as $p<0.05$. A one-phase nonlinear regression analysis (one-phase decay) was used to calculate time to steady state hypoperfusion. Statistical analysis and calculations were performed using GraphPad prism 7.0a (GraphPad Software Inc., San Diego, CA, USA). The results were presented as median values with interquartile range.

In Study II, the eyelid skin was monitored with LSCI and HSI. The LSCI speckle patterns were analyzed automatically, and the software system calculated the blood perfusion. The results are presented in arbitrary perfusion units.

To determine $sO_2$ from the HSI data, linear spectral unmixing was applied, as described above, to each pixel in the measured spectra. Calculations and statistical analysis were performed using MATLAB (The MathWorks Inc. South Natick, MA, USA). The data from LSCI and HSI were presented using median values and 95 % confidence intervals.

In Study III, the forearm skin was monitored with HSI and DRS. Spectral unmixing was performed for the DRS and HSI absorption spectra as previously described above, to determine the relative abundance (contribution) of likely absorbing chromophores (endmembers) present in the detection volume. Three models of spectral unmixing were performed:

A. Simple model, consisting of a linear sum of the spectra of $HbO_2$, HbR and scattering.
B. Full model, consisting of a linear sum of the spectra of $HbO_2$, HbR, melanin, fat and water, and scattering as endmembers which has been demonstrated to provide more accurate $sO_2$ measurements [23].
C. Baseline corrected full model, utilizing the full model applied to the baseline spectra acquired before injection to decide the baseline fractional contribution of fat and melanin. The baseline values were then fixed, and their contribution subtracted from the measured absorption spectra after injection while the fractional contribution of $HbO_2$, HbR, and water were allowed to vary after injection.

The data from HSI and DRS were presented using median values and 95 % confidence intervals.

In Study IV, the forearm skin was monitored with PAI and DRS (MoorVMS-oxy). MoorVMS-oxy automatically provided $sO_2$ in percent, as well as $HbO_2$, HbR and HbT in arbitrary units. The analysis of the photoacoustic data was performed using linear spectral unmixing as described above. Absorption spectra of five endmember spectra, for $HbO_2$, HbR, melanin, fat, and water were used. The data from DRS and PAI were presented using median values and 95 % confidence intervals.

In Study V, the finger was monitored with PAI and DRS during vascular occlusion. Absorption spectra of five endmember spectra, for $HbO_2$, HbR, melanin, fat, and water were used. A linear spectral unmixing model (described above) was used for spectral analysis. The data from PAI and DRS were presented using median values and 95 % confidence intervals.

In Study VI, calculations and statistical analysis were performed using GraphPad Prism 7.2 (GraphPad Software Inc., San Diego, CA, USA). Statistical analysis was performed using Friedman's test with Dunn's multiple comparison test.

# Ethical considerations

*Subjects and authorization*

The subjects participating in these studies were healthy volunteers and patients at the Central Hospital Växjö, and the Department of Ophthalmology, Skåne University Hospital, Sweden. The protocols for the studies were approved by the Ethics Committee at Lund University, Sweden or the Swedish Ethical Review Authority. The research complied with the principles of the Declaration of Helsinki as amended in 2013. All the subjects were thoroughly informed about the study, and the voluntary nature of participation, and gave their informed written consent before participation. Subjects unable to provide informed consent or lacking the physical or mental ability to cooperate during the local anesthesia procedure were not included in the studies.

# Overview of the novel bioimaging techniques

**Table 2. Overview of novel bioimaging techniques used in this dissertation.**

| Technique | Measured parameters | Light source | Advantages | Disadvantages |
|---|---|---|---|---|
| LSCI | Perfusion in arbitrary units | Infrared laser (785 nm) | Non-contact<br>2D maps in surface<br>Wide imaging region<br>Easy to use | Sensitive to motion artefacts<br>Limited measurement depth<br>Lack of absolute values |
| DRS | Optical spectrum | White incandescent light | Acquires high resolution spectra quickly<br>Simple commercial monitoring systems available (e.g. VMS-oxy) | Contact<br>Sensitive to motion artefacts<br>Limited measurement depth |
| HSI | Optical spectrum | White incandescent light | Non-contact<br>2D maps in surface<br>Wide imaging region | Limited measurement depth<br>Need for manual data extraction and processing |
| PAI | Optical spectrum | Multi wavelength laser and ultrasound | 3D maps in depth | Contact<br>Need for eye protection<br>Currently large equipment, portable with care<br>Need for manual data extraction and processing |

# Results and Discussion

## Monitoring spectral changes with EW-DRS

*Decrease in reflectance after epinephrine*

EW-DRS showed a clear change in reflectance after a subcutaneous injection of a local anesthetic containing epinephrine. A decrease in tissue reflectance was seen in the wavelengths 510-610 nm, a region where $HbO_2$ has an especially high absorbance. According to calculations with Dawson's erythema index, diffuse reflectance decreased over time, and reached a stable minimum after 2.6 min, and the lower level of reflectance was maintained during the rest of the measurements (20 min). A significant difference in reflectance was seen when comparing the effect of the local anesthetic containing epinephrine with that of saline ($p < 0.0001$) (Figure 12).

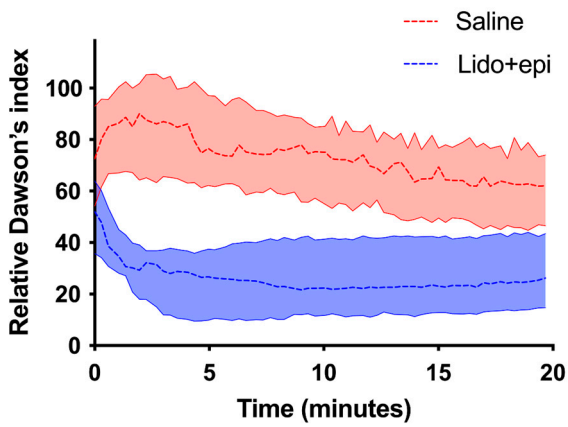


**Figure 12. Effect of injection of a local anesthetic containing epinephrine on Dawson's erythema index.**
Progression of Dawson's ertythema index over time after injection with Lidocaine with epinephrine (20 mg/ml + 12.5 µg) (denoted Lido+epi), and saline (n=8). The response in the forearm skin is expressed in percent of the baseline value of the skin before the injections, defined as 100 %. The graph is presented as median values (dashed lines) with interquartile range (shaded regions). According to a non-linear regression analysis, a stable minimum reflectance after Lido+epi was after 2.6 min.

*Spectral changes as an indicator of tissue response*

EW-DRS combines measurements from two spectrometers to obtain a broad wavelength range (450-1550 nm). When monitoring the full wavelength range a decrease in general reflectance was observed upon the injection of the local anesthetic containing epinephrine, suggesting that the broader spectrum can provide more information on the response of the tissue.

General drawbacks of DRS are the limited measurement depth and the lack of surface spatial resolution. Measurements can only be made at one point at a time. Dawson's erythema index is a validated method of measuring $HbO_2$, including information from a few wavelengths. The spectrum obtained with EW-DRS indicated the possibility of further analyzing changes in chromophores in the tissue, although this was not further explored in Study I. DRS provides a wide spectrum of wavelengths, and other methods of data analysis, such as spectral unmixing, could be explored in future studies.

## Surface-resolved mapping with HSI

*Perfusion after injection of a local anesthetic containing epinephrine*

In Study II, LSCI and HSI were used in a complementary way to visualize the effect of epinephrine in the eyelid skin. A central decrease in perfusion could be seen at the site of injection with LSCI. According to an exponential fit, half-maximum was found after 34 s, and the full effect after 115 s, after which no further decrease was observed. The minimum level of stable perfusion was found to be 35 % of the initial value. The decrease in perfusion was slower further away from the injection site, and at 4 mm from the injection site a spatially dependent half-maximum effect was observed after 231 s.

The measurement depth of LSCI is approximately 1 mm, and thus the observed hemostatic effect was primarily that of the action of epinephrine on the surface of the skin. It was thus not possible in the present study to deduce the hemostatic effect deeper down in the eyelid such as on the orbicularis oculi muscle.

*Oxygen saturation in the eyelid after injection of a local anesthetic containing epinephrine*

Measurements were also performed with HSI after the administration of a local anesthetic containing epinephrine in the eyelid skin. A slight gradual reduction in $sO_2$ was seen over 7 min period (Figure 13) . In this case, an exponential fit yielded a time to half-maximum effect of 205 s, compared to 34 s when perfusion was

measured with LSCI. Hypothetically a decrease in perfusion may not affect $sO_2$ instantly, but lead to a delayed reduction over time. Eyelid $sO_2$ was only reduced by 11 %, possibly due to the well vascularized nature of the human eyelid.

The patients recruited for Study II were those planned to undergo blepharoplasty. In all other studies included in this dissertation, the subjects were healthy volunteers in an attempt to create a homogeneous study group. The group of patients in Study II was thus much more heterogeneous, and included smokers and patients taking medication for diabetes, hypertension, and blood thinners. The study group of 9 patients was relatively small, and the results were thus expressed as median values and 95 % confidence intervals. On the other hand, the group in Study II represents real patients undergoing eyelid procedures, as many of these patients are elderly with comorbidities. Larger groups should be included in future studies to confirm the results and to allow specific group analysis.

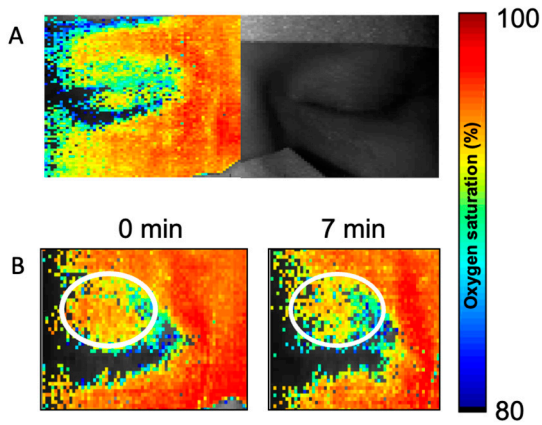


**Figure 13. Representative example of a baseline hyperspectral image and the effect of epinephrine on oxygen saturation.**
(A) Oxygen saturation map (left) and regular image (right) at baseline prior to injection with a local anesthetic containing epinephrine. (B) Oxygen saturation maps right after injection (left) and after 7 min (right). Red indicates higher oxygenation and blue lower oxygenation, see bar to the right.

*The effect of epinephrine in local anesthetics on oxygen saturation*

In the early 20th century, before new synthetic local anesthetics had been developed, some cases of ischemic necrosis were observed, and were assumed to depend on high levels of epinephrine. Therefore, surgeons have been taught that local anesthetics containing epinephrine should not be injected into organs with end arteries [106]. Since then there has been much debate on the safety of using epinephrine in organs such as the ear, nose, penis, and digits [107]. However, many

studies have shown that local anesthetics containing epinephrine in digital blocks have several advantages, including safer usage, longer duration of anesthesia, reduced anesthetic volume, and minimized bleeding, and the old dogma is nowadays considered refuted [107-109].

The eyelid is a well-perfused region of the body [110], and is therefore a forgiving region for reconstructive surgery. The survival of flaps in reconstructive surgery is dependent on the perfusion and oxygenation of the tissue. In a previous study carried out on pigs by our research group, a local anesthetic containing epinephrine was injected in the base of a full thickness eyelid flap (10 mm x 30 mm). It was found that the perfusion remaining in the flap was 20 % of the original, suggesting that it is safe to use anesthetics containing epinephrine in eyelid flaps [97]. In Study II, $sO_2$ was found to be only slightly decreased in the eyelid after the injection of an anesthetic containing epinephrine, despite a decrease in perfusion. This also indicates that the use of epinephrine in the eyelid is safe. However, the results must be confirmed over a longer observational time in future studies.

## Depth-resolved mapping with PAI

*Identification of endmembers in different skin layers*

The ability of PAI to create depth-resolved images of the tissue was evaluated in Studies IV and V. Five known endmember spectra were included in the analysis, representing absorption by $HbO_2$, HbR, melanin, fat, and water. The spectral unmixing of these endmembers showed differences in the molecular composition between the skin layers. Melanin dominated the absorption in the epidermis, while a prominent signal from $HbO_2$ was detected further down in the superficial dermis, i.e., in the superficial vascular plexus. A clear signal from $HbO_2$ was seen in the hypodermis where the deep vascular plexus is located (Figure 14).

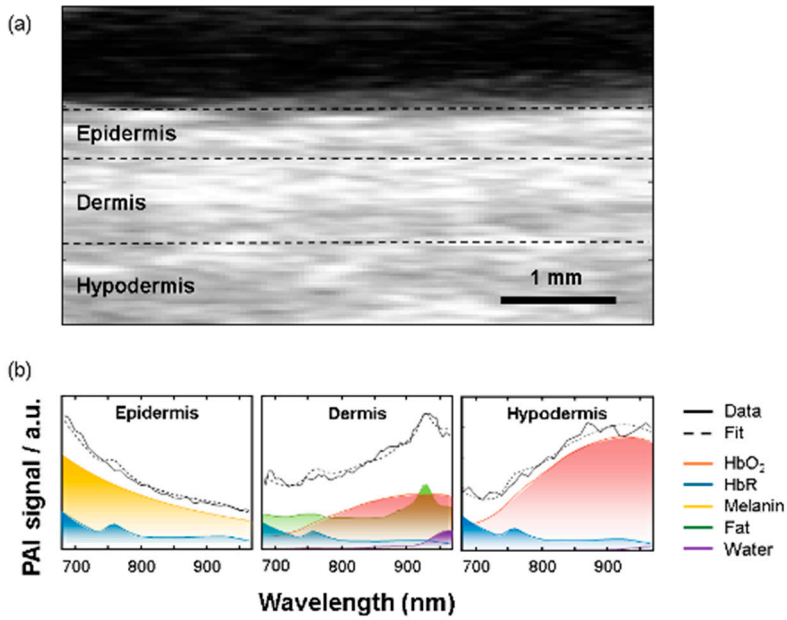


**Figure 14. Photoacoustic image of the skin in which the different skin layers and endmembers are identified.**
(A). A representative example of a cross-section at a depth in tissue acquired with ultrasound where the different tissue layers, epidermis, dermis and hypodermis are identified. (B). Results from the spectral unmixing analysis from the three skin layers, where both the measured spectrum and the total fit, as well as the individual spectral contribution from each endmember, are shown.

*Spatially resolved oxygen saturation in forearm skin*

In Study IV, PAI was used to monitor the effect of a local anesthetic with epinephrine. The anesthetic was injected into the forearm skin, targeting the superficial vascular plexus. Thereafter, a decrease in HbT in the superficial dermis was observed with PAI. In addition, the level of $HbO_2$ decreased, while the level of HbR increased, which led to a gradual decrease in $sO_2$. This is consistent with what would be expected after vasoconstriction induced by epinephrine. The measurements of HbT deeper down in the hypodermis showed a stable signal, indicating that $sO_2$ was unaffected at this depth. This demonstrates the ability of PAI in monitoring $sO_2$ with high spatial resolution. A small number of subjects (n=7) were included in this study, which could have influenced the results, however, the clear reduction in $HbO_2$ agrees with the expected results.

*Melanin as a stable chromophore*

While clear changes were seen in $HbO_2$ levels in Study IV, the absolute level of melanin should not change due to injection of a local anesthetic. Melanin was thus

used to validate the spectral unmixing results. The analysis showed that the amount of melanin remained stable during the measurements, which also indicates that PAI is not sensitive to measurement artefacts due to motion or laser fluctuations.

*Depth-dependent changes in oxygenation after injection with local anesthetic containing epinephrine*

In study IV, a decrease in $sO_2$ was found in the dermis with PAI after the injection of local anesthetics containing epinephrine in the forearm skin. A single exponential function of 123 s was fitted to the change in $sO_2$, which indicates that the time to maximum vasoconstrictive effect is approximately 2 min. When measuring $sO_2$ with DRS an initial decrease was seen during the initial 40 s, followed by an increase with a time constant of 109 s, similar to the time constant obtained with PAI (Figure 15). Earlier studies by our group have shown similar results after the injection of anesthetics containing epinephrine. This could be due to the "window effect", described below, where blanching of the skin causes a deeper penetration of the signal down to the deeper vascular plexus, where perfusion is not affected in the same way [102].

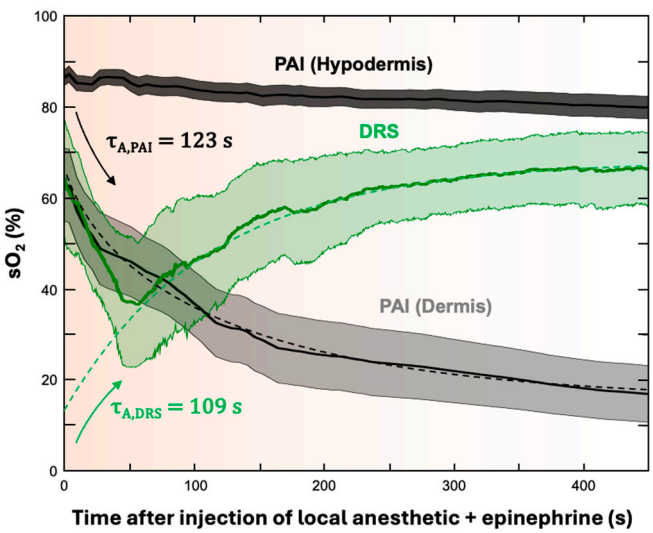


**Figure 15. Evolution of $sO_2$ after injection of an anesthetic with epinephrine measured with PAI and DRS.**
Progression of $sO_2$ over time measured with PAI and DRS. The black trace represents $sO_2$ in the hypodermis, while the gray trace represents $sO_2$ in the dermis measured by PAI. The green trace shows $sO_2$ measured by DRS. Applying a single exponential fit (dotted lines) to the traces, we obtain time constants which characterize the rate at which the epinephrine effect takes place. A paradoxical increase in $sO_2$ is seen as measured with DRS, but with a similar time constant to that measured in the dermis with PAI. This is interpreted as being due to the window effect, as explained above. The data is presented as median values (solid lines) with 95 % confidence intrervals (shaded areas).

*Depth-resolved oxygenation during vascular occlusion*

In study VI, $sO_2$ was monitored with DRS (moorVMS-OXY) and in depth with PAI, during vascular occlusion of a finger. The three skin layers could be delineated with PAI, and the dominating chromophores in the layers could be identified. Melanin could be identified in the epidermis, and more HbT, in terms of $HbO_2$ and HbR, was found lower down in the dermis. After occlusion, $sO_2$ decreased in all layers except the epidermis, where there is no vascular supply. The greatest decrease in $sO_2$ was observed in the dermis, where the superficial plexus is situated. However, the decrease in $sO_2$ was greater and faster when measured with DRS than with PAI. The measurement depth of DRS was ≈1 mm, which is the location of the superficial plexus. The mapping of $sO_2$ as a function of depth by PAI indicates that oxygenation is affected differently in the skin layers during vascular occlusion (Figure 16).

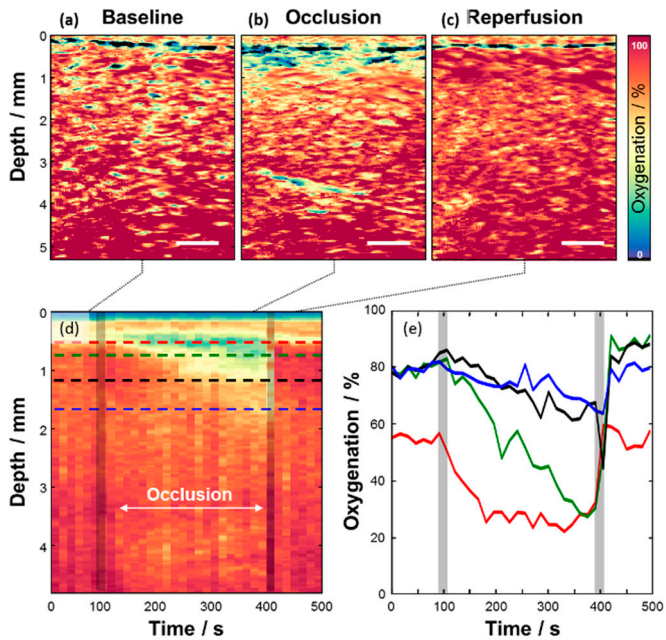


**Figure 16. Evolution of $sO_2$ during finger occlusion measured with PAI.**
(A-C). $SO_2$ maps of the tissue to a depth of 5 mm at baseline, occlusion and reperfusion. (D) A time progression of the depth profile, capturing how $sO_2$ changes in time at different depths. (E) Progression of how $sO_2$ changes from baseline, through occlusion of the finger, to reperfusion at different depths (dotted lines indicated in D).

# Evaluation of spectral unmixing

*Spectral unmixing with the simple and complete model*

Spectral unmixing has been evaluated in several of the studies included in this dissertation, and the analytical process has progressed over time. In Study III, human forearm skin was studied with HSI and a custom-built DRS instrument in order to further develop the method of analysis. HSI spectra were analyzed using several spectral unmixing models, for example, a simple model with few endmembers ($HbO_2$ and HbR), and the complete model with many endmembers as well as a baseline fixed model.

When using the simple model, $sO_2$ was found to be underestimated across all parameters in the baseline measurements. Increasing the number of endmembers in the full model led to an improved and more evenly distributed fit (Figure 17) and more importantly results that agree more with what is expected from a physiological perspective. In the baseline fixed full model, it was assumed that endmembers such as melanin and fat would be unaffected by the injection of epinephrine, which is why the contribution from these specific endmembers were fixed to the values obtained at baseline.

Similar to the results in Study I, the DRS spectra in study III showed spectral changes (concerning $sO_2$), directly after epinephrine injection that changed gradually over the measurement period (5 min). After injection of the anesthetic with epinephrine, an immediate increase in $sO_2$ to 98.4 % of the baseline was seen, followed by a decrease to 56.2 % after 5 min. An exponential fit gave a time constant of 1-1.5 min, indicating how rapidly epinephrine acts in the tissue.

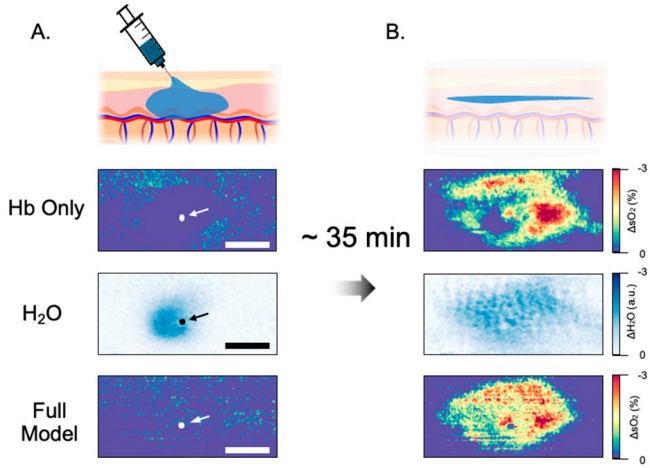


**Figure 17. Heat maps of oxygenation after the injection of an anesthetic containing epinephrine obtained with HSI.**
Heat maps at 0 min (A) and 35 min (B) after injection with local anesthetic containing epinephrine. The 1st row shows diffusion of water in relation to the injection site during a time period of 35 min. A comparison of the results depicting the change in $sO_2$ ($\Delta sO_2$) when applying the different models in which the simple model can generate regions where there is no change in $sO_2$ after 35 min (2nd row). Applying the full model where also the effect of water is accounted for (3rd row) yields a more even distribution of $\Delta sO_2$ (4th row).

*Hyperemic effect of local anesthesia*

A hyperemic response has been observed in some studies directly after administration of a local anesthetic with epinephrine [73, 111]. Lidocaine is known to cause vasodilation at high concentrations [83], but in Study III a hyperemic effect was also seen after the injection of the saline, which likely has other explanations. A chemical response to tissue damage caused by the needle, leading to histamine release from mast cells, is a well-known phenomenon. To evaluate the chemical reaction in the tissue in future studies, a reference site could be used where the needle penetrates the subcutaneous skin without injecting any liquid.

Another hypothesis could be that a presumed vasodilation in fact is a misinterpretation of $sO_2$ due to a changing environment caused by the injection. The water content of the local anesthetic could be a possible source of error due to the change in absorption characteristics. In the baseline fixed model in Study III the hyperemic effect after injection was not seen. Therefore, not taking water in account during analysis of the spectral changes could lead to overestimation of $sO_2$ why a model including more endmembers could be preferable.

*Monitoring $sO_2$ in a changing environment*

Irrespective of the imaging technique chosen, analyzing the data and interpreting the results and their correlation with physiological and pathological processes can pose a significant challenge. The biological reaction after the injection of epinephrine is complex, and many different processes will be involved, all of which vary between individuals. Bickler et al. performed a study using several commercial cerebral oximeters and found a considerable variation in reading errors between the meters in subjects with cerebral hypoxia [112]. This could be related to variations between subjects, and the ratio between arterial and venous blood, which was not considered in these commercial devices. In order to measure variations in different regions of a tissue, bioimaging techniques with spatial resolution, and the possibility to adjust data processing following changes in the environment would be required.

Attempts have been made in several studies to measure the vasoconstrictive effect of epinephrine in skin, with varying results [73, 111, 113, 114]. Analyzing $sO_2$ in a changing environment can be challenging due to the varying relative abundance of key chromophores. When adding water, as in the context of a local anesthetic, the absorption by longer wavelengths will increase, leading to the risk of misimpression of $sO_2$ values if not taking water in to account in the analysis. A calibration-free method, such as spectral unmixing, including water as an endmember, could perhaps provide more reliable values.

*Spectral coloring*

The phenomenon of "spectral coloring" is a known limitation when analyzing spectra from different depths of tissue, such as in Study IV and V. As light propagates through tissue, different wavelengths are absorbed to various degrees by the chromophores in the skin layers. Consequently, fewer wavelengths are detected deeper in the tissue, and the comparison of the abundance of an endmember can therefore be misleading. Blood, for example, is one of the strongest absorbers of light. However, as $sO_2$ is calculated as the ratio of $HbO_2$ to HbT at a given depth, the results are less likely to be affected by spectral coloring.

In Study V, spectral coloring was investigated by measuring the spectrum above in and under an artery. The high $sO_2$ level in the artery contrasted with lower $sO_2$ levels in the surrounding tissue. Given that hemoglobin is a strong light absorber, it would be reasonable to expect that light passing through an artery would significantly change the spectrum experienced by the underlying tissue layers. However, the $sO_2$ levels remain unchanged at similar depths in a nearby tissue segment without an artery suggested that spectral coloring had little effect in this case.

*The window effect*

A challenge when using one-point measurements (DRS) or measurements with surface resolution (LSCI, HSI) is that we cannot precisely know what depth is being measured. In the different skin layers, there is a varying amount of blood present due to vascular anatomy. An injection with a local anesthetic containing epinephrine leads to a vasoconstriction and therefore less blood in the superficial skin. When illuminating this tissue there is a possibility that the incoming light will penetrate to a different depth, due to reduced absorption by blood in the superficial skin. Deeper in the skin the deep vascular plexus is found, and is presumably not affected by the epinephrine at the same extent and can thus indicate a higher perfusion or $sO_2$ than expected. This is referred to as "the window effect" (Figure 18) and has been suspected in Study IV and in earlier studies by our research group [102]. A technique with spatial resolution in depth, such as PAI, could help overcome this potential source of error and risk of misinterpretation in measurements.

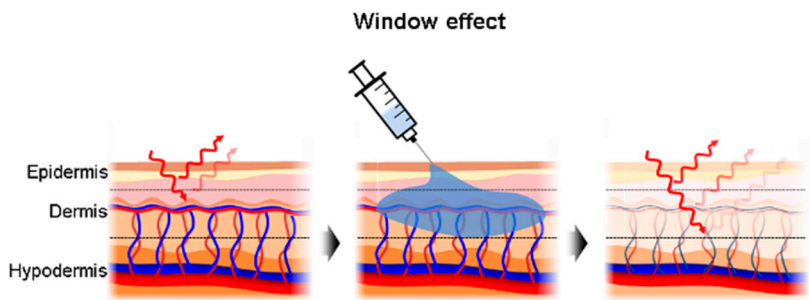


**Figure 18. Illustration of how the window effect affects the penetration of light and the interpretation of perfusion and $sO_2$.**
Left: Skin monitored with DRS, with a measuring depth of ≈1 mm. Center: Injection of a local anesthetic with epinephrine. Right: Less blood is present in the region due to vasoconstriction, which leads to a deeper penetration of the light, in this case targeting the lower dermal plexus which could lead to misinterpretation of the results.

# Time to full effect of epinephrine

Today, physicians use local anesthesia not only in outpatient surgery, but also to improve analgesia in procedures performed under general anesthesia [91]. Epinephrine is often added to local anesthetics to induce vasoconstriction and reduce bleeding during surgery. Although local anesthesia has been studied and used for over a century, many questions remain regarding the optimal waiting time

before commencing surgery, specifically regarding the vasoconstrictive effect of epinephrine.

In this dissertation, different ways of studying the effects of local anesthesia with epinephrine have been discussed. In Studies I-IV, epinephrine reached full effect after about 2 min, which is in good agreement with clinical experience, especially in oculoplastic surgery. However, there are still conflicting opinions regarding the time required to achieve stable vasoconstrictive effects following infiltration of a local anesthetic with epinephrine. This information is important, since a prolonged waiting time after administration of a local anesthetic with epinephrine would imply a need for changed preoperative routines.

Technical challenges, together with biological disparities, imply difficulties in measuring the effect of epinephrine. In studies measuring intraoperative bleeding, the time to minimum perfusion in the eyelid was described to be 7 min and in the upper limb 25 min [93, 111]. Several studies in which different imaging techniques were used in different anatomical sites have showed considerable variation in the maximum effect of epinephrine in a local anesthetic (0-30 min) [73, 85, 102, 111, 113, 114]. If the optimal waiting time is longer than a few minutes, a change in most surgical routines must be considered. There may be many explanations of the disparities between studies, such as different anatomical sites, the volume and concentration of anesthetics and the technique used to inject. Furthermore, it is not always possible to compare the results from studies using different imaging techniques.

In the studies included in this dissertation show the importance of spatially resolved imaging when imaging human skin has been exemplified. A surface or depth resolved image gives further understanding of the anatomical changes in tissue due to hypoperfusion. Further studies are needed, to further investigate the question and understand the effect of epinephrine in local anesthetics.

# Pain on injection, and the onset and duration of buffered local anesthetics

*Pain on administration of buffered local anesthetics*

In Study VI, three different preparations of buffered and non-buffered local anesthetics were compared concerning pain on injection, and the onset and duration of anesthesia. Injection with buffered lidocaine with epinephrine (pH ≈7.4) was the least painful, and the subjects assessed the pain to be 1.5 on the NRS. Injection of

non-buffered lidocaine with epinephrine (pH ≈4.2) was significantly more painful with a NRS score of 4.5 ($p<0.01$). The injection of non-buffered lidocaine (pH ≈6.0) was also more painful than buffered lidocaine with epinephrine with NRS 3.5 ($p<0.05$). Thus, the results of this study show that pain on injection was significantly lower when administering buffered lidocaine with epinephrine, than non-buffered lidocaine with epinephrine with a higher concentration (Figure 19).

Solutions with lower pH levels contribute to increased pain through two distinct mechanisms. Firstly, the acidity of the solution leads to a burning sensation upon infiltration into tissues with a more neutral pH. Secondly, at lower pH levels, less of the anesthetic exists in its active, freely diffusible form, resulting in a prolonged onset time for anesthesia [95].

A factor that could further affect the results of Study VI is the potential pain reduction during injection by warming the solution beforehand, which was done for all the solutions in the study [115].

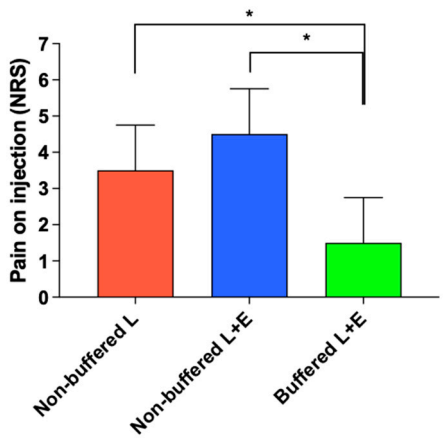


**Figure 19. Pain on injection with three different local anesthetic solutions determined with a numerical rating scale (NRS).**
Buffered local anesthetic containing epinephrine (Buffered L+E) was the least painful on administration, with a median of 1.5. This was significantly lower than a non-buffered local anesthetic (Non-buffered L+E) with higher concentration of lidocaine with epinephrine and a non-buffered solution with lidocaine alone (Non-buffered L) (*$p<0.05$).

### *Onset and duration of buffered local anesthesia*

In study VI, the onset of anesthesia was just around 2 min and was similar for the three preparations. There was no statistically significant difference between the onset of anesthesia with the three agents, although the results indicate a slight clinical difference. The duration of anesthesia was much longer with the local

anesthetics containing epinephrine; 5.6 h (2.3 to 8.8 h) for buffered lidocaine with epinephrine and 6.6 h (4.3 to 9.8 h) for non-buffered lidocaine with epinephrine (higher concentration), than for lidocaine alone (1.3 h, range 0.8 to 3.3 h) (Figure 20). Although it was statistically significant, the difference between the buffered anesthetic and the non-buffered lidocaine with epinephrine has limited clinical significance, particularly for surgical procedures lasting less than 5.6 h. The results indicate that a buffered local anesthetic with lower concentration of lidocaine and epinephrine is just as effective as lidocaine with epinephrine with a higher concentration, while causing less pain on injection.

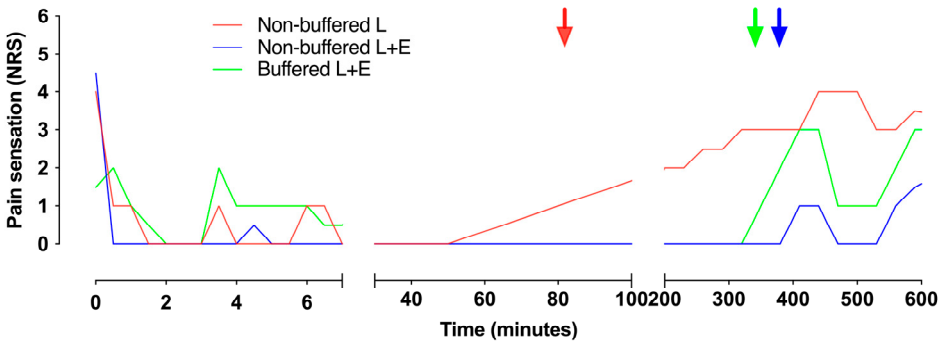


**Figure 20. Onset and duration of buffered and non-buffered local anesthetics.**
Onset and duration of anesthesia after administering three local anesthetics in the forearm of healthy subjects, measured in terms of pain using the numerical rating scale. The time to onset was similar for the preparations, just under 2 min. The preparation buffered to the physiological pH of the tissue (Buffered L+E) and the non-buffered preparation (Non-buffered L+E) had long durations, around 6 h, which differed significantly ($p<0.01$) compared to lidocaine alone (Non-buffered L).

### *Clinical practice of buffering local anesthetics*

Although local anesthesia is associated with a low rate of complications and has a well-studied safety profile [116], administration is often feared by patients; in some cases, even more than the surgical procedure itself. The acidity of the solution and the injection technique can influence the pain experienced during injection. Additionally, several factors affect the onset and duration of local anesthesia, including the drug's binding affinity to Na+ channels, its lipophilicity, the pH of the tissue, the presence of vasoconstrictors, as well as the concentration, and volume of the injected drug [83]. Buffered local anesthetics cause less pain during administration, making them a good choice for pediatric patients, adults with special needs, and procedures involving sensitive areas such as the face [7]. A higher concentration of epinephrine may be a better choice during surgical procedures when bleeding must be minimized, or when the patient is taking anticoagulants.

Buffered lidocaine is believed to have a short shelf life of only one day, due to falling concentrations of the active substances at room temperature [117]. Larson et al. studied the shelf life of a buffered local anesthetic stored in a refrigerator and found that the concentrations of epinephrine and lidocaine were 99 % and 97 %, respectively, after two weeks [118]. As buffered preparations have distinct advantages for patients, storage in a refrigerator may allow their more widespread use.

Additional studies are required to investigate the effect of local anesthetics in other parts of the body and the effects deeper in the tissue. It would also be interesting to investigate the characteristics of other local anesthetics, such as bupivacaine. Bupivacaine and lidocaine are often used together to take advantage of the more rapid onset of anesthesia with lidocaine and the longer duration of bupivacaine. However, when comparing the onset of action of lidocaine with epinephrine, bupivacaine with epinephrine, and mixtures of these local anesthetics Collins et al. found no significant difference. Thus, although bupivacaine has a longer duration, the clinical advantage of this can be discussed depending on the length of the surgery [91].

In Study VI, no reference area outside the anesthetized area, or negative control was used (for example, an injection of saline). However, pinching the subjects' skin repeatedly over a few hours without local anesthetics was not considered ethically acceptable.

It would have been interesting to examine all the preparations at different concentrations, including both buffered and non-buffered solutions. However, the limited area of the forearm and ethical considerations regarding the number of injections per subject made it impractical to study all the preparations at different concentrations. Tweezers were used to pinch the skin to determine the level of pain by using NRS. However, this method may have some variability and provides no information on the pain response at deeper levels in the skin. It was therefore not possible to draw any profound conclusions regarding the onset and duration of anesthesia in the subcutaneous tissue. Furthermore, no surgical procedure was performed, which hypothetically could change the properties of the tissue and the anesthetic effect.

# Conclusions

The conclusions drawn from the studies included in this dissertation are summarized below.

- DRS has the ability to monitor change in perfusion and $sO_2$ in the skin, but does not provide any spatial resolution.
- HSI is able to create a 2D map of the skin with a detailed view of $sO_2$.
- PAI has the ability to identify the different layers of the skin and produce a depth-resolved 3D map of $sO_2$.
- Spectral unmixing can be applied to spectra obtained with any of the techniques: DRS, HSI and or PAI, to determine the contribution of specific chromophores in a tissue.
- Epinephrine in a local anesthetic reaches maximum effect in the forearm and eyelid skin in approximately 2 min, as measured by DRS, HSI, and PAI. A 2 min wait after injection ensures maximum hypoperfusion before eyelid surgery.
- A buffered local anesthetic with low concentrations of lidocaine and epinephrine provides similar anesthetic effects and duration as an unbuffered solution with higher concentration, but with less injection pain. Using a buffered local anesthetic for surgery up to 5 h could be preferable to reduce patient pain and stress.

# Future perspectives

Novel bioimaging techniques are rapidly evolving to meet the growing demand for more precise and clinically assessable tissue imaging. This dissertation describes non-invasive imaging techniques for monitoring $sO_2$ in a model of hypoperfusion. DRS, HSI, and PAI have many advantages over historically used techniques as they all use a broad spectral range allowing a detailed view of tissue viability and the analysis of changes in chromophores in the tissue. HSI and PAI offer spatially resolved imaging of both the skin surface and its deeper layers, providing comprehensive information on the composition of the tissue.

A limitation of the studies described above is the limited number of subjects, and therefore non-parametric statistical methods were used. Mostly healthy subjects were included, and due to the small study groups no sub-group analysis was possible. It would be interesting to study the effect of hypoperfusion in smokers or subjects with diabetes, especially using PAI to determine whether there are any differences in vascular response in the various skin levels compared that to healthy individuals.

Spectral coloring has been discussed as a possible limitation when measuring spectral changes at depth with PAI. The optical fluence (energy disposition) is not evenly distributed within the anatomy of the skin, and the absorption of different chromophores is wavelength-dependent in the different skin layers. However, spectral coloring was not found to be a problem in Study V when measuring the spectral changes above and under an artery in the tissue. Despite this, spectral coloring is an issue that should be investigated in the future.

When monitoring conscious subjects, motion artefacts are inevitable. In some of these studies, it was necessary to exclude some subjects due to excessive motion artifacts, which led to data loss. For techniques providing spatial resolution, such as HSI and PAI, motion correction techniques could enhance image resolution. The use of machine-learning-based motion correction software could perhaps improve data quality and represent a promising direction for future technical advancements.

In many of the studies included in this dissertation, two different techniques were employed on the same subjects. This approach allowed for a more extensive

evaluation of the results and helped identify the advantages and drawbacks of each technique. Combining two imaging techniques with different properties could be a promising approach for advancing clinical methodologies. For example, the combination of LSCI and HSI, in Study II, offered an appealing method for simultaneous measurements perfusion and $sO_2$. This integrated approach could be valuable in for example reconstructive surgery. Monitoring both perfusion and oxygenation has the potential to enhance surgical outcomes in many procedures, and may also contribute to the development of new surgical techniques. Furthermore, being able to image both the surface and depth of a tissue simultaneously with HSI and PAI, would help us gain a much more detailed understanding of tissue viability and structure. The combination of techniques could be useful, for example, in cases of skin burns and in skin tumor diagnostics.

In conclusion, novel bioimaging techniques are still in the early stages of development, but have great potential for clinical use. Some technical challenges remain, such as motion artifacts, spectral coloring, and monitoring in a changing environment. However, once these issues are resolved and clinical implementation is achieved, we can look forward to advanced monitoring and comprehensive assessment of tissue.

# Populärvetenskaplig sammanfattning

I sjukvården är det viktigt att kunna mäta syresättning och blodflöde för att ta reda på hur vävnaden och patienten mår. Att kunna mäta den lokala syresättning i vävnaden är extra viktigt vid till exempel rekonstruktiv plastikkirurgi, brännskador och sår orsakade av diabetes. Traditionellt sett har man bedömt vävnaden genom att känna och titta på hudens temperatur och färg, men detta är grova mått och kräver stor klinisk erfarenhet. Tidigare har metoder som innehåller till exempel fluorescerande och radioaktiva ämnen använts för att mäta blodflöde och syresättning i vävnad men dessa tekniker är invasiva och opraktiska i den kliniska vardagen. Därtill har de flesta tidigare avbildningsteknikerna varit baserade på mätningar i en punkt, med begränsad information om den omgivande vävnaden på ytan och djupet.

Syftet med denna avhandling var att utforska nya icke-invasiva avbildningstekniker inkluderande diffus reflektans spektroskopi, hyperspektral avbildning och fotoakustisk avbildning för att mäta syresättningen i hud vid nedsatt blodflöde.

Två metoder användes för att åstadkomma nedsatt blodflöde i huden:

1. Injektion i huden med lokalbedövning som innehåller adrenalin och som därmed drar samman kärlen i huden.
2. Strypning av blodflödet i ett finger med en liten blodtrycksmanschett.

Lokalbedövning syftar till att bedöva området där operationen ska ske och med tillägg av adrenalin kan man även få en blodstillande effekt samtidigt som bedövningen verkar längre i området. Trots att adrenalin används flitigt i lokalbedövningar finns det motstridiga studier om hur lång tid man bör vänta innan man får full effekt av adrenalinet.

Då lokalbedövning är en sur vätska gör det ont när man injicerar. Man kan genom att tillsätta bikarbonat (buffring) göra lokalbedövningen mindre sur och därmed minska smärtan vid injektionen. Ett ytterligare syfte med avhandlingen var att undersöka egenskaper så som smärta vid injektion, tillslagstid och duration av en buffrad lokalbedövning jämfört med en icke-buffrad, samt att bestämma tiden till full effekt av adrenalinet i lokalbedövningen.

I den första studien användes diffus reflektans spektroskopi med utökat våglängdsspann. Efter en injektion med lokalbedövning med adrenalin i underarmen kunde vi se en minskning av syresatt blod i området. Ytterligare förändringar i ett bredare våglängdsspann kunde identifieras som tecken på att även andra substanser i vävnaden förändrades efter injektionen.

I den andra studien studerades huden på ögonlocket efter injektion av lokalbedövning med adrenalin med hyperspektal avbildning och laser speckle contrast imaging. Med hjälp av hyperspektral avbildning kunde en karta över syresättningen i ögonlocket skapas och denna visade en liten minskning till 89 % av ursprungsvärdet. Blodflödet i ögonlocket minskade däremot mer, till 35 % av ursprungsvärdet. Att syresättningen endast sjunker lite kan förklaras av att ögonområdet är väldigt kärlrikt och att vävnaden därmed klarar syresättningen trots nedsatt blodflöde. Vi kunde dra slutsatsen att lokalbedövning med adrenalin är säkert att använda i ögonlocket.

I den tredje studien gjordes en utvidgad analys av syresättningen efter injektion av lokalbedövning med adrenalin i underarmen. Vi kunde konstatera att det är svårt att analysera vävnadens beståndsdelar i en föränderlig miljö så som när man injicerar lokalbedövning med adrenalin som till exempel innehåller stor mängd vatten. I denna studie visade det sig vara viktigt att ta med vatten i beräkningarna som gjordes med hjälp av en metod som kallas ”spectral unmixing”.

I den fjärde och femte studien använde vi fotoakustisk avbildning för att skapa en karta av syresättningen på djupet i huden på underarm och i ett finger. Vi kunde se att syresättningen sjönk mest i de ytliga delarna av huden där injektionen med adrenalin var placerad och där ett ytligt nätverk av kärl är lokaliserat. Längre ner i huden var syresättningen mindre påverkad av injektionen. När en liten blodtrycksmanschett ströp blodflödet i fingret kunde vi se att förändringen av syresatt blod förändrades olika på olika djup i huden. Kraftigast minskning av syresatt blod förelåg i de ytliga delarna av huden.

I den sjätte studien jämfördes en buffrad lokalbedövning med en icke-buffrad lokalbedövning med högre koncentration avseende smärta vid injektion, tillslagstid och verkningstid. Resultatet visade att injektionssmärtan var lägre med den buffrade lokalbedövningen och att verkningstiden för de båda beredningarna var lika med eller mer än fem timmar. Vår slutsats är därmed att en buffrad lösning är fördelaktig ur smärtsynpunkt för operationer som varar mindre än fem timmar. Buffrad lokalbedövning kan vara fördelaktigt vid behandling av barn eller vuxna med särskilda behov samt i kroppsdelar som är speciellt känsliga, tex ansiktet.

Flera nya avbildningstekniker har utvärderats i avhandlingen. Dessa tekniker har alla fördelen av att använda ett brett våglängdsområde vilket möjliggör en detaljerad

analys av vävnaden vad gäller syresättning men också avseende annat innehåll i vävnaden så som melanin, vatten och fett. Hyperspektral och fotoakustisk avbildning ger en karta med detaljerad information om vävnaden och är därför lovande tekniker för framtida klinisk användning.

Sammanfattningsvis visade resultaten i studie I-IV att den maximala effekten av adrenalin i lokalbedövning är efter ungefär två minuter vilket stämmer bra med flera andra liknande studier samt även klinisk erfarenhet av användning av lokalbedövning i ögonområdet. Studierna i avhandlingen har också visat fördelar med tekniker som ger en spatial upplösning på ytan och på djupet eftersom det ger bättre förståelse för förändringar som sker i vävnaden. Fler studier behövs i framtiden för att ytterligare fördjupa kunskapen om avbildningstekniker och för att förstå effekten av adrenalin i lokalbedövning.

# Acknowledgments

A heartfelt thank you to everyone who has contributed to my dissertation and my personal life. A special thanks to those mentioned below, your support has been invaluable.

*My supervisors*

**Rafi Sheikh,** principal supervisor and associate professor. Always there for honest advice and with the ability to always see the opportunities for new projects. Need help choosing a tech gadget, a flashlight, or even the perfect type of rice? Rafi's your man! Thank you for believing in me, giving me the opportunity to start my research, and for your support in the clinic as well.

**Malin Malmsjö,** co-supervisor and professor. A true superwoman and inspiration. With you, everything is possible and fun! You have created a fantastic team that works together with a wonderful forward-thinking spirit. Thank you for taking me under your wing!

**Karl Engelsberg,** co-supervisor and associate professor. A wise colleague who always takes the time to answer questions. You have been a great support to me in both research and clinical work. Additionally, you have a special fascination for Budapest-cake, which, despite its name, originates from Småland.

**Nina Reistad,** co-supervisor and associate professor. You have been with me since the beginning of my doctoral studies, offering valuable advice and encouragement. Always prepared, you carry an energy bar in your bag for those late study sessions with me. Nina earned her Ph.D. in Experimental Physics from Lund University in 1987, becoming the youngest person in Sweden to do so - a true inspiration.

**Aboma Merdasa,** co-supervisor and PhD. A true optimist who is always ready to provide technical support, no matter the time or place - whether it's the middle of the night, at the playground with your children, or during a vacation halfway around the world. Thank you for coming to Växjö to assist with the research and for your continuing encouragement.

*My research colleagues in Lund*

**Johan Albinsson,** a steady support, always available when you need help. You have a remarkable ability to remain calm, think logically, and provide careful reviews.

**Magdalena Naumovska,** an intelligent research colleague who inspires and always offers a friendly hug and advice along the way. Thank you for carefully reading my dissertation and coming up with good suggestions.

**Johanna Vennström Berggren,** an incredibly kind research colleague. In addition, a skilled oculoplastic surgeon with great pedagogical skills. A special thank you for traveling to Växjö to assist with the research.

**Kajsa Tenland,** a helpful research colleague, who has given a lot of good advice along the way. Shares my interest in pediatric ophthalmology and I hope for fun collaborations in the future.

**Jenny Hulth,** a supportive colleague, whose stunning illustrations have not only enhanced my work but have also helped the rest of the team in their research. In addition, an impressive mother of three managing to commute to from Copenhagen to Lund.

**Ulf Dahlstrand,** a skilled oculoplastic surgeon and researcher with a knack for always having a funny remark ready.

**Bodil Gesslein,** a confident and friendly research colleague, thanks for the all the good advice and help along the way!

**Nils Gustafsson,** a warm and friendly research colleague. Thank you for your dedication with our collaborative research project.

**Julio Hérnandez-Palacios,** engineer and research collaborator from Olso, Norway. Thank you for valuable technical support and assistance with the research.

**Magnus Cintio and Tobias Erlöv,** engineers and research colleagues at LTH who give good advice and perspective on the technical front.

**Linn Engqvist,** a lively and quick-thinking research colleague who guides us on the best shopping routes and is always there to help.

**Magne Stridh,** a talented singer and friendly research colleague who has now also started his career as an ophthalmologist.

Other members of the research group: **Joakim Thylefors, Hanna-Maria Öhnell, Sofia Paulsson, Olof Neumann and Jens Nääv Ottosson.** Thank you for all your help along the way and for contributing to the positive atmosphere in our research team.

**Helen Shepard,** thank you for invaluable and honest help with the language during my time as a PhD student.

*Colleagues in Växjö, Lund and Stockholm*

**Sivert Eriksson,** my dear friend and teacher in oculoplastic surgery who is no longer with us. Even in retirement, you traveled from Skåne to Växjö for several years to educate us. You were always there for a hug and still inspire. I miss you.

**Paula Silvert,** current head of the eye clinic in Växjö/Ljungby. Thank you for supporting me in completing my PhD studies and for your consistent positivity and curiosity.

**Karin Fafner Wallentén,** PhD and former head of the eye clinic in Växjö/Ljungby. A wise and experienced colleague who paved the way for PhD students in Växjö. Thank you for supporting my decision to pursue research.

**Gabor Koranyi,** PhD and former head of the eye clinic in Växjö/Ljungby and a true optimist. Thank you for promoting research and for hiring me at the eye clinic.

To all current and former **colleagues and clinic management in Lund** - Thank you for fostering a fantastic research culture and a welcoming atmosphere!

**Jonas Blohmé,** an experienced and skilled oculoplastic surgeon who inspires and always lightens the mood with a funny story. Thank you for recommending me!

**Sven Hector,** an incurable optimist, a great support and my lunch companion at the clinic. You impressively manage pediatric ophthalmology, cataract surgery, research, family of four children and a self-sufficient household.

**Malin Fredholm Langlo,** my dear friend and former roommate with whom I shared many fun moments. I miss you a lot now that you have started your own private clinic, but luckily, we still get to see you a lot for lunches.

**Pernilla Rosenqvist and Ludvig Magnusson,** friendly and competent colleagues who helped with the research in Växjö and Lund. Many thanks!

**Ingrid Reitan,** my mentee and future shooting star. You have remarkable pedagogical skills and bring joy to everyone around you. Additionally, thank you for participating in and contributing to future research projects.

**Magnus Johansson,** a very friendly colleague who is always ready to help and take on challenges. You are already a skilled oculoplastic surgeon despite not having completed your residency. Thank you for participating in and contributing to future research projects.

**Karin Hjelmberg,** an invaluable nurse in Växjö and friend who is always ready to help. She solves all issues easily and efficiently with a smile.

**Elin Bohman,** a fantastic and wise colleague at St. Erik's Eye Hospital. Thank you for the great advice along the way. I look forward to fun collaborations in the future.

**Colleagues at the eye clinic in Växjö**, former and current colleagues including medical doctors, nurses, assistant nurses and secretaries who have been there to educate, organize and support. Thank you all for your help, and for contributing to the wonderful group atmosphere at the eye clinic in Växjö.

*Research colleagues in Region Kronoberg*

**Carina Elmqvist,** professor and head of the research unit in Växjö. You make everything seem possible. Thank you for your inspiration and for the support throughout my research.

**Birgitta Grahn,** associate professor and former head of research at the research unit in Växjö. You have done a remarkable job establishing a research culture now flourishing in Region Kronoberg. Thank you also for the enjoyable conversations over the fence.

**Dorthe Geisler, Sofi Tschannen and Amanda Gustafsson,** you are a dream team! Thank you for your invaluable help and support during my PhD studies.

**Anna Lindskog and Anna Bennesved,** competent and delightful PhD colleagues with whom I had a lot of fun organizing the “doktorand kollegiet” in Region Kronoberg.

To **all other colleagues at the research unit in Region Kronoberg,** thank you for pleasant conversations and advice along the way.

*My friends*

**Gerd Sandman, Emelie Lind, Maria Järbur,** my closest friends from medical school. Thank you for all the wonderful times we've shared, both in the past and looking ahead.

To all my **new and old friends in Sweden, Norway, Denmark, South Africa and Australia,** though I can't name everyone individually, none of you are forgotten. We've shared countless memorable moments, and your friendship and support are truly priceless.

*My family*

**Mutti,** my grandmother who is no longer with us. Your joyful laugh and mischievous spirit made you a true role model. You are always with me.

**Farmor Gunnel,** my grandmother who has also passed. You were so happy when I entered the medical field, thrilled that I had "gotten through the eye of the needle". You are always with me.

**Mamma Tina,** "Lycklig och glad" (happy and joyful) - there is no more positive and loving person in the world. Your support means everything to me. I love you!

**Pappa Pär,** you have always had big ambitions and have shown us that anything is possible. Thank you for your constant presence and wise, grounded advice. I love you!

**Lena, Torsten and Nina with family,** thank you for all the support and help with babysitting, painting our house and all fun times we share.

**Ia and Måns,** my sister and brother-in-law, you are always there to lend a hand. You have given me a lot of support and good advice along the way. I am so grateful for you both!

**Crille and Kathy,** my brother and sister-in-law living in England. Your assistance and humor are always just a phone call away, I deeply value your support and love.

My amazing nephews, **Fabian, Teodor, Disa, Alexander, Sebastian and Stefan**. You are truly one of a kind, with the whole world ahead of you. You are so precious to me!

**Johan,** my dear husband and my rock. Life with you is everything I could ever wish for. Thank you for your endless support and patience along the way. I promise to pitch in more with the dishes, laundry and the children from now on. I love you!

**Lovisa, Oscar and Walter,** our wonderful children. Each of you is perfect in your own unique way. I love you endlessly.

# References


1. Lintzeri, D.A., et al., *Epidermal thickness in healthy humans: a systematic review and meta-analysis.* J Eur Acad Dermatol Venereol, 2022. **36**(8): p. 1191-1200.
2. Fernandez-Flores, A., *Regional Variations in the Histology of the Skin.* Am J Dermatopathol, 2015. **37**(10): p. 737-54.
3. Skobe, M. and M. Detmar, *Structure, function, and molecular control of the skin lymphatic system.* J Investig Dermatol Symp Proc, 2000. **5**(1): p. 14-9.
4. Yousef, H., et al., *Anatomy, Skin (Integument), Epidermis*, in *StatPearls*. 2024: Treasure Island (FL).
5. Safran, T., et al., *Efficacy of Local Anesthesia in the Face and Scalp: A Prospective Trial.* Plast Reconstr Surg Glob Open, 2019. **7**(5): p. e2243.
6. Becker, D.E. and K.L. Reed, *Local anesthetics: review of pharmacological considerations.* Anesth Prog, 2012. **59**(2): p. 90-101; quiz 102-3.
7. Won, S.Y., et al., *Two-point discrimination values vary depending on test site, sex and test modality in the orofacial region: a preliminary study.* J Appl Oral Sci, 2017. **25**(4): p. 427-435.
8. Eriksson, S., J. Nilsson, and C. Sturesson, *Non-invasive imaging of microcirculation: a technology review.* Med Devices (Auckl), 2014. **7**: p. 445-52.
9. Cracowski, J.L. and M. Roustit, *Human Skin Microcirculation.* Compr Physiol, 2020. **10**(3): p. 1105-1154.
10. Egginton, S., *Invited review: activity-induced angiogenesis.* Pflugers Arch, 2009. **457**(5): p. 963-77.
11. Levick, J.R., *An introduction to cardiovascular physiology*. 2010, London: Hodder Arnold.
12. Heistad, D.D. and F.M. Abboud, *Factors that influence blood flow in skeletal muscle and skin.* Anesthesiology, 1974. **41**(2): p. 139-56.
13. Charkoudian, N., *Skin blood flow in adult human thermoregulation: how it works, when it does not, and why.* Mayo Clin Proc, 2003. **78**(5): p. 603-12.
14. Braverman, I.M. and A. Yen, *Ultrastructure of the human dermal microcirculation. II. The capillary loops of the dermal papillae.* J Invest Dermatol, 1977. **68**(1): p. 44-52.

15. Braverman, I.M. and A. Keh-Yen, *Ultrastructure of the human dermal microcirculation. III. The vessels in the mid- and lower dermis and subcutaneous fat.* J Invest Dermatol, 1981. **77**(3): p. 297-304.
16. Alghoul, M., et al., *Eyelid reconstruction.* Plast Reconstr Surg, 2013. **132**(2): p. 288e-302e.
17. Dailey, R.A. and J.L. Wobig, *Eyelid anatomy.* J Dermatol Surg Oncol, 1992. **18**(12): p. 1023-7.
18. Chen, Y., et al., *Free Flap Monitoring Using Near-Infrared Spectroscopy: A Systemic Review.* Ann Plast Surg, 2016. **76**(5): p. 590-7.
19. Pickard, A., W. Karlen, and J.M. Ansermino, *Capillary refill time: is it still a useful clinical sign?* Anesth Analg, 2011. **113**(1): p. 120-3.
20. Repez, A., D. Oroszy, and Z.M. Arnez, *Continuous postoperative monitoring of cutaneous free flaps using near infrared spectroscopy.* J Plast Reconstr Aesthet Surg, 2008. **61**(1): p. 71-7.
21. Berggren, J., et al., *Reperfusion of Free Full-Thickness Skin Grafts in Periocular Reconstructive Surgery Monitored Using Laser Speckle Contrast Imaging.* Ophthalmic Plast Reconstr Surg, 2021. **37**(4): p. 324-328.
22. Berggren, J.V., et al., *Blood Perfusion of Human Upper Eyelid Skin Flaps Is Better in Myocutaneous than in Cutaneous Flaps.* Ophthalmic Plast Reconstr Surg, 2022. **38**(2): p. 166-169.
23. Merdasa, A., et al., *Oxygen saturation mapping during reconstructive surgery of human forehead flaps with hyperspectral imaging and spectral unmixing.* Microvasc Res, 2023. **150**: p. 104573.
24. Ansson, C.D., et al., *Blood perfusion in Hewes tarsoconjunctival flaps in pigs measured by laser speckle contrast imaging.* JPRAS Open, 2018. **18**: p. 98-103.
25. Tenland, K., et al., *Successful Free Bilamellar Eyelid Grafts for the Repair of Upper and Lower Eyelid Defects in Patients and Laser Speckle Contrast Imaging of Revascularization.* Ophthalmic Plast Reconstr Surg, 2021. **37**(2): p. 168-172.
26. Memarzadeh, K., et al., *Large Eyelid Defect Repair Using a Free Full-Thickness Eyelid Graft.* Plast Reconstr Surg Glob Open, 2017. **5**(7): p. e1413.
27. McDonald, H.M., K.A. McDonald, and H. McDonald, *The free bilamellar autograft (FBA) procedure: A comprehensive case series of an alternative surgical approach to reconstruction of large eyelid defects.* Front Surg, 2023. **10**: p. 1038952.
28. Rowan, M.P., et al., *Burn wound healing and treatment: review and advancements.* Crit Care, 2015. **19**: p. 243.
29. Kagan, R.J., et al., *Surgical management of the burn wound and use of skin substitutes: an expert panel white paper.* J Burn Care Res, 2013. **34**(2): p. e60-79.
30. Kaiser, M., et al., *Noninvasive assessment of burn wound severity using optical technology: a review of current and future modalities.* Burns, 2011. **37**(3): p. 377-86.

31. Claes, K.E.Y., et al., *Evidence Based Burn Depth Assessment Using Laser-Based Technologies: Where Do We Stand?* J Burn Care Res, 2021. **42**(3): p. 513-525.
32. Wang, Q., et al., *In vivo burn scar assessment with speckle decorrelation and joint spectral and time domain optical coherence tomography.* J Biomed Opt, 2023. **28**(12): p. 126001.
33. Hinchliffe, R.J., et al., *IWGDF guidance on the diagnosis, prognosis and management of peripheral artery disease in patients with foot ulcers in diabetes.* Diabetes Metab Res Rev, 2016. **32 Suppl 1**: p. 37-44.
34. Argarini, R., et al., *Optical coherence tomography: a novel imaging approach to visualize and quantify cutaneous microvascular structure and function in patients with diabetes.* BMJ Open Diabetes Res Care, 2020. **8**(1).
35. Weingarten, M.S., et al., *Diffuse near-infrared spectroscopy prediction of healing in diabetic foot ulcers: a human study and cost analysis.* Wound Repair Regen, 2012. **20**(6): p. 911-7.
36. Jayachandran, M., et al., *Critical Review of Noninvasive Optical Technologies for Wound Imaging.* Adv Wound Care (New Rochelle), 2016. **5**(8): p. 349-359.
37. Sloan, G.M. and J.F. Reinisch, *Flap physiology and the prediction of flap viability.* Hand Clin, 1985. **1**(4): p. 609-19.
38. Nitzan, M., I. Nitzan, and Y. Arieli, *The Various Oximetric Techniques Used for the Evaluation of Blood Oxygenation.* Sensors (Basel), 2020. **20**(17).
39. Scheeren, T.W., P. Schober, and L.A. Schwarte, *Monitoring tissue oxygenation by near infrared spectroscopy (NIRS): background and current applications.* J Clin Monit Comput, 2012. **26**(4): p. 279-87.
40. Valentinuzzi, M.E. and A.J. Kohen, *James Clerk Maxwell, Kirchhoff's Laws, and their implications on modeling physiology.* IEEE Pulse, 2013. **4**(2): p. 40-6.
41. Wukitsch, M.W., et al., *Pulse oximetry: analysis of theory, technology, and practice.* J Clin Monit, 1988. **4**(4): p. 290-301.
42. Jacques, S.L., *Optical properties of biological tissues: a review.* Phys Med Biol, 2013. **58**(11): p. R37-61.
43. Keller, M.D., et al., *Skin colour affects the accuracy of medical oxygen sensors.* Nature, 2022. **610**(7932): p. 449-451.
44. Sinaki, F.Y., et al., *Ethnic disparities in publicly-available pulse oximetry databases.* Commun Med (Lond), 2022. **2**: p. 59.
45. Kulcke, A., et al., *A compact hyperspectral camera for measurement of perfusion parameters in medicine.* Biomed Tech (Berl), 2018. **63**(5): p. 519-527.
46. Holmer, A., et al., *Hyperspectral imaging in perfusion and wound diagnostics - methods and algorithms for the determination of tissue parameters.* Biomed Tech (Berl), 2018. **63**(5): p. 547-556.
47. Heeman, W., et al., *Clinical applications of laser speckle contrast imaging: a review.* J Biomed Opt, 2019. **24**(8): p. 1-11.

48. Hoshi, Y. and Y. Yamada, *Overview of diffuse optical tomography and its clinical applications.* J Biomed Opt, 2016. **21**(9): p. 091312.
49. Amaro, E., Jr. and G.J. Barker, *Study design in fMRI: basic principles.* Brain Cogn, 2006. **60**(3): p. 220-32.
50. Briers, J.D. and A.F. Fercher, *Retinal blood-flow visualization by means of laser speckle photography.* Invest Ophthalmol Vis Sci, 1982. **22**(2): p. 255-9.
51. Cheng, H., Y. Yan, and T.Q. Duong, *Temporal statistical analysis of laser speckle images and its application to retinal blood-flow imaging.* Opt Express, 2008. **16**(14): p. 10214-9.
52. Yamamoto, Y., et al., *Laserflowgraphy: a new visual blood flow meter utilizing a dynamic laser speckle effect.* Plast Reconstr Surg, 1993. **91**(5): p. 884-94.
53. Della Rossa, A., et al., *Alteration of microcirculation is a hallmark of very early systemic sclerosis patients: a laser speckle contrast analysis.* Clin Exp Rheumatol, 2013. **31**(2 Suppl 76): p. 109-14.
54. Parthasarathy, A.B., et al., *Laser speckle contrast imaging of cerebral blood flow in humans during neurosurgery: a pilot clinical study.* J Biomed Opt, 2010. **15**(6): p. 066030.
55. Hecht, N., et al., *Laser speckle imaging allows real-time intraoperative blood flow assessment during neurosurgical procedures.* J Cereb Blood Flow Metab, 2013. **33**(7): p. 1000-7.
56. Ansson, C.D., et al., *Perfusion in Upper Eyelid Flaps: Effects of Rotation and Stretching Measured With Laser Speckle Contrast Imaging in Patients.* Ophthalmic Plast Reconstr Surg, 2020. **36**(5): p. 481-484.
57. Tenland, K., et al., *Blood Perfusion in Rotational Full-Thickness Lower Eyelid Flaps Measured by Laser Speckle Contrast Imaging.* Ophthalmic Plast Reconstr Surg, 2020. **36**(2): p. 148-151.
58. Lindahl, F., E. Tesselaar, and F. Sjoberg, *Assessing paediatric scald injuries using Laser Speckle Contrast Imaging.* Burns, 2013. **39**(4): p. 662-6.
59. Mennes, O.A., et al., *Assessment of microcirculation in the diabetic foot with laser speckle contrast imaging.* Physiol Meas, 2019. **40**(6): p. 065002.
60. Myers, D.E., et al., *Noninvasive method for measuring local hemoglobin oxygen saturation in tissue using wide gap second derivative near-infrared spectroscopy.* J Biomed Opt, 2005. **10**(3): p. 034017.
61. Glennie, D.L., J.E. Hayward, and T.J. Farrell, *Modeling changes in the hemoglobin concentration of skin with total diffuse reflectance spectroscopy.* J Biomed Opt, 2015. **20**(3): p. 035002.
62. Egawa, M., et al., *Regional difference of water content in human skin studied by diffuse-reflectance near-infrared spectroscopy: consideration of measurement depth.* Appl Spectrosc, 2006. **60**(1): p. 24-8.

63. Phelps, J.E., et al., *Rapid ratiometric determination of hemoglobin concentration using UV-VIS diffuse reflectance at isosbestic wavelengths.* Opt Express, 2010. **18**(18): p. 18779-92.
64. de Boer, L.L., et al., *Fat/water ratios measured with diffuse reflectance spectroscopy to detect breast tumor boundaries.* Breast Cancer Res Treat, 2015. **152**(3): p. 509-18.
65. Evers, D.J., et al., *Optical sensing for tumor detection in the liver.* Eur J Surg Oncol, 2013. **39**(1): p. 68-75.
66. Langhout, G.C., et al., *Nerve detection during surgery: optical spectroscopy for peripheral nerve localization.* Lasers Med Sci, 2018. **33**(3): p. 619-625.
67. Aggarwal, S.L.P. and F.A. Papay, *Applications of multispectral and hyperspectral imaging in dermatology.* Exp Dermatol, 2022. **31**(8): p. 1128-1135.
68. Schulz, T., et al., *Diagnostical accuracy of hyperspectral imaging after free flap surgery.* J Plast Surg Hand Surg, 2023. **58**: p. 48-55.
69. Chiang, N., et al., *Evaluation of hyperspectral imaging technology in patients with peripheral vascular disease.* J Vasc Surg, 2017. **66**(4): p. 1192-1201.
70. Khaodhiar, L., et al., *The use of medical hyperspectral technology to evaluate microcirculatory changes in diabetic foot ulcers and to predict clinical outcomes.* Diabetes Care, 2007. **30**(4): p. 903-10.
71. Nouvong, A., et al., *Evaluation of diabetic foot ulcer healing with hyperspectral imaging of oxyhemoglobin and deoxyhemoglobin.* Diabetes Care, 2009. **32**(11): p. 2056-61.
72. Yudovsky, D., A. Nouvong, and L. Pilon, *Hyperspectral imaging in diabetic foot wound care.* J Diabetes Sci Technol, 2010. **4**(5): p. 1099-113.
73. Thiem, D.G.E., et al., *Hyperspectral Imaging to Study Dynamic Skin Perfusion after Injection of Articaine-4% with and without Epinephrine-Clinical Implications on Local Vasoconstriction.* J Clin Med, 2021. **10**(15).
74. Chin, M.S., et al., *Hyperspectral Imaging for Burn Depth Assessment in an Animal Model.* Plast Reconstr Surg Glob Open, 2015. **3**(12): p. e591.
75. Promny, D., et al., *Evaluation of hyperspectral imaging as a modern aid in clinical assessment of burn wounds of the upper extremity.* Burns, 2022. **48**(3): p. 615-622.
76. Wang, L.V., *Multiscale photoacoustic microscopy and computed tomography.* Nat Photonics, 2009. **3**(9): p. 503-509.
77. Wu, Z., et al., *In vivo dual-scale photoacoustic surveillance and assessment of burn healing.* Biomed Opt Express, 2019. **10**(7): p. 3425-3433.
78. Taruttis, A., et al., *Optoacoustic Imaging of Human Vasculature: Feasibility by Using a Handheld Probe.* Radiology, 2016. **281**(1): p. 256-63.
79. Yang, M., et al., *Synovial Oxygenation at Photoacoustic Imaging to Assess Rheumatoid Arthritis Disease Activity.* Radiology, 2023. **306**(1): p. 220-228.

80. Ali, J., et al., *Near-Infrared Spectroscopy (NIRS) for Cerebral and Tissue Oximetry: Analysis of Evolving Applications.* J Cardiothorac Vasc Anesth, 2022. **36**(8 Pt A): p. 2758-2766.
81. Ruetsch, Y.A., T. Boni, and A. Borgeat, *From cocaine to ropivacaine: the history of local anesthetic drugs.* Curr Top Med Chem, 2001. **1**(3): p. 175-82.
82. Holmdahl, M.H., *Xylocain (lidocaine, lignocaine), its discovery and Gordh's contribution to its clinical use.* Acta Anaesthesiol Scand Suppl, 1998. **113**: p. 8-12.
83. Michel-Levy, J.M., *Pharmacokinetics and Pharmacodynamics of Local Anesthetics*, in *Topics in Local Anesthetics*. 2020, IntechOpen: Rijeka. p. 1-16.
84. Yang, X., et al., *A review of the mechanism of the central analgesic effect of lidocaine.* Medicine (Baltimore), 2020. **99**(17): p. e19898.
85. Larrabee, W.F., Jr., B.J. Lanier, and D. Miekle, *Effect of epinephrine on local cutaneous blood flow.* Head Neck Surg, 1987. **9**(5): p. 287-9.
86. Brown, R.S. and N.L. Rhodus, *Epinephrine and local anesthesia revisited.* Oral Surg Oral Med Oral Pathol Oral Radiol Endod, 2005. **100**(4): p. 401-8.
87. Niwa, H., et al., *Cardiovascular response to epinephrine-containing local anesthesia in patients with cardiovascular disease.* Oral Surg Oral Med Oral Pathol Oral Radiol Endod, 2001. **92**(6): p. 610-6.
88. Knoll-Kohler, E., et al., *Cardiohemodynamic and serum catecholamine response to surgical removal of impacted mandibular third molars under local anesthesia: a randomized double-blind parallel group and crossover study.* J Oral Maxillofac Surg, 1991. **49**(9): p. 957-62.
89. Rhodus, N.L. and J.W. Little, *Dental management of the patient with cardiac arrhythmias: an update.* Oral Surg Oral Med Oral Pathol Oral Radiol Endod, 2003. **96**(6): p. 659-68.
90. Bajwa, M.S., et al., *How long to wait after local infiltration anaesthesia: systematic review.* BJS Open, 2023. **7**(5).
91. Collins, J.B., J. Song, and R.C. Mahabir, *Onset and duration of intradermal mixtures of bupivacaine and lidocaine with epinephrine.* Can J Plast Surg, 2013. **21**(1): p. 51-3.
92. Collin, J.R.O. and G. Rose, *Plastic and orbital surgery*. Fundamentals of clinical ophthalmology. 2001, London: BMJ Books.
93. Hult, J., et al., *A waiting time of 7 min is sufficient to reduce bleeding in oculoplastic surgery following the administration of epinephrine together with local anaesthesia.* Acta Ophthalmol, 2018. **96**(5): p. 499-502.
94. McKee, D.E., et al., *Achieving the optimal epinephrine effect in wide awake hand surgery using local anesthesia without a tourniquet.* Hand (N Y), 2015. **10**(4): p. 613-5.
95. Christoph, R.A., et al., *Pain reduction in local anesthetic administration through pH buffering.* Ann Emerg Med, 1988. **17**(2): p. 117-20.

96. Frank, S.G. and D.H. Lalonde, *How acidic is the lidocaine we are injecting, and how much bicarbonate should we add?* Can J Plast Surg, 2012. **20**(2): p. 71-3.
97. Sheikh, R., et al., *Optimal Epinephrine Concentration and Time Delay to Minimize Perfusion in Eyelid Surgery: Measured by Laser-Based Methods and a Novel Form of Extended-Wavelength Diffuse Reflectance Spectroscopy.* Ophthalmic Plast Reconstr Surg, 2018. **34**(2): p. 123-129.
98. Bargman, H., *Laser classification systems.* J Clin Aesthet Dermatol, 2010. **3**(10): p. 19-20.
99. Lu, G. and B. Fei, *Medical hyperspectral imaging: a review.* J Biomed Opt, 2014. **19**(1): p. 10901.
100. Hennessy, R., et al., *Effect of probe geometry and optical properties on the sampling depth for diffuse reflectance spectroscopy.* J Biomed Opt, 2014. **19**(10): p. 107002.
101. Dawson, J.B., et al., *A theoretical and experimental study of light absorption and scattering by in vivo skin.* Phys Med Biol, 1980. **25**(4): p. 695-709.
102. Sheikh, R., et al., *Hypoperfusion following the injection of epinephrine in human forearm skin can be measured by RGB analysis but not with laser speckle contrast imaging.* Microvasc Res, 2019. **121**: p. 7-13.
103. Attia, A.B.E., et al., *A review of clinical photoacoustic imaging: Current and future trends.* Photoacoustics, 2019. **16**: p. 100144.
104. Yao, J. and L.V. Wang, *Photoacoustic tomography: fundamentals, advances and prospects.* Contrast Media Mol Imaging, 2011. **6**(5): p. 332-45.
105. Sheikh, R., et al., *Clinical Translation of a Novel Photoacoustic Imaging System for Examining the Temporal Artery.* IEEE Trans Ultrason Ferroelectr Freq Control, 2019. **66**(3): p. 472-480.
106. Lalonde, D. and A. Martin, *Epinephrine in local anesthesia in finger and hand surgery: the case for wide-awake anesthesia.* J Am Acad Orthop Surg, 2013. **21**(8): p. 443-7.
107. Sylaidis, P. and A. Logan, *Digital blocks with adrenaline. An old dogma refuted.* J Hand Surg Br, 1998. **23**(1): p. 17-9.
108. Ilicki, J., S. Bruchfeld, and T. Djarv, *Can epinephrine therapy be detrimental to patients with hypertrophic cardiomyopathy with hypotension or cardiac arrest? A systematic review.* Eur J Emerg Med, 2019. **26**(3): p. 150-157.
109. Lalonde, D., et al., *A multicenter prospective study of 3,110 consecutive cases of elective epinephrine use in the fingers and hand: the Dalhousie Project clinical phase.* J Hand Surg Am, 2005. **30**(5): p. 1061-7.
110. Codner, M.A., et al., *Upper and lower eyelid reconstruction.* Plast Reconstr Surg, 2010. **126**(5): p. 231e-245e.
111. McKee, D.E., et al., *Optimal time delay between epinephrine injection and incision to minimize bleeding.* Plast Reconstr Surg, 2013. **131**(4): p. 811-814.

112. Bickler, P.E., J.R. Feiner, and M.D. Rollins, *Factors affecting the performance of 5 cerebral oximeters during hypoxia in healthy volunteers.* Anesth Analg, 2013. **117**(4): p. 813-823.
113. Ghali, S., et al., *Effects of lidocaine and epinephrine on cutaneous blood flow.* J Plast Reconstr Aesthet Surg, 2008. **61**(10): p. 1226-31.
114. O'Malley, T.P., et al., *Effect of local epinephrine on cutaneous bloodflow in the human neck.* Laryngoscope, 1995. **105**(2): p. 140-3.
115. Colaric, K.B., D.T. Overton, and K. Moore, *Pain reduction in lidocaine administration through buffering and warming.* Am J Emerg Med, 1998. **16**(4): p. 353-6.
116. Alam, M., et al., *Safety of Local Intracutaneous Lidocaine Anesthesia Used by Dermatologic Surgeons for Skin Cancer Excision and Postcancer Reconstruction: Quantification of Standard Injection Volumes and Adverse Event Rates.* Dermatol Surg, 2016. **42**(12): p. 1320-1324.
117. Stewart, J.H., G.W. Cole, and J.A. Klein, *Neutralized lidocaine with epinephrine for local anesthesia.* J Dermatol Surg Oncol, 1989. **15**(10): p. 1081-3.
118. Larson, P.O., et al., *Stability of buffered lidocaine and epinephrine used for local anesthesia.* J Dermatol Surg Oncol, 1991. **17**(5): p. 411-4.

Printed by Media-Tryck, Lund 2024 NORDIC SWAN ECOLABEL 3041 0903

# About the author

**JOSEFINE BUNKE** received her medical degree from Lund University in 2011. She currently works as an ophthalmologist at the Central Hospital of Växjö, specializing in oculoplastic surgery and pediatric ophthalmology. Her primary research focus is in the field of oculoplastic surgery and bioimaging techniques. This thesis explores novel non-invasive bioimaging techniques and the use of spectral information to monitor oxygen saturation and perfusion in human skin.

LUND UNIVERSITY

FACULTY OF MEDICINE

Department of Clinical Sciences, Lund

Lund University, Faculty of Medicine
Doctoral Dissertation Series 2024:119
ISBN 978-91-8021-615-9
ISSN 1652-8220